Inhibition of spindle extension through the yeast S phase checkpoint is coupled to replication fork stability and the integrity of centromeric DNA

Jeff Julius[a], Jie Peng[b], Andrew McCulley[b], Chris Caridi[a], Remigiusz Arnak[b], Colby See[a], Constance I. Nugent[a], Wenyi Feng[b], and Jeff Bachant[a,*]

[a]Department of Molecular Cell Systems Biology, University of California, Riverside, Riverside, CA 92521; [b]Department of Biochemistry and Molecular Biology, State University of New York Upstate Medical University, Syracuse, NY 13210

ABSTRACT **Budding yeast treated with hydroxyurea (HU) activate the S phase checkpoint kinase Rad53, which prevents DNA replication forks from undergoing aberrant structural transitions and nuclease processing. Rad53 is also required to prevent premature extension of the mitotic spindle that assembles during a HU-extended S phase. Here we present evidence that checkpoint restraint of spindle extension is directly coupled to Rad53 control of replication fork stability. In budding yeast, centromeres are flanked by replication origins that fire in early S phase. Mutations affecting the Zn^{2+}-finger of Dbf4, an origin activator, preferentially reduce centromere-proximal origin firing in HU, corresponding with suppression of *rad53* spindle extension. Inactivating *Exo*1 nuclease or displacing centromeres from origins provides a similar suppression. Conversely, short-circuiting Rad53 targeting of Dbf4, Sld3, and Dun1, substrates contributing to fork stability, induces spindle extension. These results reveal spindle extension in HU-treated *rad53* mutants is a consequence of replication fork catastrophes at centromeres. When such catastrophes occur, centromeres become susceptible to nucleases, disrupting kinetochore function and spindle force balancing mechanisms. At the same time, our data indicate centromere duplication is not required to stabilize S phase spindle structure, leading us to propose a model for how monopolar kinetochore-spindle attachments may contribute to spindle force balance in HU.**

Monitoring Editor
Orna Cohen-Fix
National Institutes of Health

Received: Mar 15, 2019
Revised: Aug 14, 2019
Accepted: Sep 4, 2019

INTRODUCTION

The S phase checkpoint is a conserved signal transduction pathway enabling eukaryotic cells to tolerate DNA replication stress. In budding yeast, checkpoint signaling is initiated when impediments to DNA synthesis cause single-stranded DNA (ssDNA) to accumulate at replication forks, leading to activation of the central checkpoint kinase Mec1 (reviewed in Pardo *et al.*, 2017). Mec1 then acts through the mediator Mrc1 to phosphorylate and activate the effector kinase Rad53 (Sanchez *et al.*, 1996; Osborn and Elledge, 2003). In broad terms, Rad53 controls two seemingly distinct forms of regulation within the S phase checkpoint. First, Rad53 mediates responses that, collectively, allow DNA synthesis to continue despite perturbations to replication forks. These responses include delaying the temporal program of replication origin (*ORI*) firing (Santocanale and Diffley, 1998; Shirahige *et al.*, 1998), activating the protein kinase Dun1 to upregulate ribonucleotide reductase (RNR; Zhou and Elledge, 1993; Zhao and Rothstein, 2002), and directly regulating the stability and exonucleolytic susceptibility of DNA replication forks (Lopes *et al.*, 2001; Sogo *et al.*, 2002; Katou *et al.*, 2003; Cotta-Ramusino *et al.*, 2005; Bermejo *et al.*, 2011; Rossi *et al.*, 2015; Colosio *et al.*, 2016). Failure to execute these forms of DNA replication control has severe consequences. *rad53* mutants treated with

This article was published online ahead of print in MBoC in Press (http://www.molbiolcell.org/cgi/doi/10.1091/mbc.E19-03-0156) on September 11, 2019.

*Address correspondence to: Jeff Bachant (jeffbach@ucr.edu).

Abbreviations used: AK, artificial K; AUC, area under the curve; *CEN*, centromeric; DDK, Dbf4-dependent kinase; Fkh, Forkhead; HU, hydroxyurea; K, kinetochore; MT, microtubule; NLS, nuclear localization sequence; NZ, nocodazole; *ORI*, replication origin; pre-RC, prereplication complex; RNR, ribonucleotide reductase; SAC, spindle assembly checkpoint; SC, synthetic complete; SPB, spindle pole body; ssDNA, single-stranded DNA; WT, wild type; YPD, yeast extract/peptone/dextrose.

the RNR inhibitor hydroxyurea (HU) activate *ORI*s throughout the genome, greatly increasing the number of forks experiencing replication challenge (Feng *et al.*, 2006). Many of these forks undergo reversal or collapse, corresponding with DNA damage and accumulation of ssDNA (Lopes *et al.*, 2001; Sogo *et al.*, 2002; Feng *et al.*, 2006, 2011).

A second role for Rad53 is to maintain the capacity for accurate chromosome segregation once impediments to DNA replication have been resolved. Budding yeast undergo a closed mitosis, and commitment to spindle pole body (SPB) duplication and intranuclear spindle assembly occurs as cells initiate S phase (Hartwell, 1976). In rich media, S phase is typically complete before SPBs separate and spindle assembly begins. However, when DNA replication is extended by HU, this relative timing is altered such that S phase checkpoint-proficient cells arrest mitotic progression having assembled an ~1 to 2-μm bipolar spindle (Byers and Goetsch, 1974; referred to here as the S phase spindle). In contrast, S phase checkpoint mutants undergo premature spindle extension in HU (Allen *et al.*, 1994; Weinert *et al.*, 1994; Navas *et al.*, 1995; Alcasabas *et al.*, 2001), but otherwise remain blocked in the cell cycle, eventually completing bulk genome duplication (Desany *et al.*, 1998; Feng *et al.*, 2009). *rad53* mutants recovering from HU ultimately fail to biorient sister chromatids on the spindle, indicating a profound defect in their ability to resume chromosome segregation (Feng *et al.*, 2009).

While a molecular understanding of Rad53 control of DNA replication has progressed, checkpoint mechanisms enforcing the block to spindle extension have remained less defined. A clarifying realization was that spindle extension in HU-treated *rad53* mutants does not reflect premature anaphase entry (Krishnan *et al.*, 2004; Bachant *et al.*, 2005). In yeast, the metaphase to anaphase transition is controlled through proteolysis of the anaphase inhibitor Pds1 (Cohen-Fix *et al.*, 1996). Pds1 degradation triggers sister chromatid disjunction, after which spindles extend to 8–10 μm (Ciosk *et al.*, 1998; Jensen *et al.*, 2001; Severin *et al.*, 2001b; Khmelinskii *et al.*, 2009; Lianga *et al.*, 2018). In contrast, *rad53* spindles extend only partially in HU (3–7 μm), displaying cycles of extension, breakage, and collapse (Bachant *et al.*, 2005) and spindle extension occurs even though Pds1 is stabilized (Feng *et al.*, 2009; Palou *et al.*, 2017). Moreover, Pds1 is not required for short spindle arrest in HU (Yamamoto *et al.*, 1996). A careful kinetic analysis showed HU-treated *pds1* mutants do eventually exhibit premature spindle extension, but only after two-thirds of the genome has been duplicated (Clarke *et al.*, 2001). In comparison, spindles extend as soon as they are formed in *mec1* and *rad53* mutants. These observations suggest that delayed chromosome segregation at the S phase checkpoint involves two sequential responses. The first is a rapidly acting, Pds1-independent response that maintains the structural stability and/or appropriate length regulation of the S phase spindle. The second response is Pds1-dependent and becomes operational after substantial genome duplication has been achieved.

Prior work in our labs has focused on the mechanism of the rapidly acting block to spindle extension in HU. Spindle length regulation reflects a balance between microtubule (MT) motors that extend the central spindle and a counteracting, inward-directed, force (Saunders *et al.*, 1997). In budding yeast, considerable evidence suggests this inward force is generated through amphitelic attachment of sister kinetochores (Ks) and the tensile properties of the C-loop, an elastic pericentromeric (*CEN*) domain (Bouck and Bloom, 2007; Yeh *et al.*, 2008; Stephens *et al.*, 2011; Nannas *et al.*, 2014). Notably, all 16 yeast *CEN*s are flanked by *ORI*s that fire in HU-treated cells (Raghuraman *et al.*, 2001). In previous work, we therefore proposed that one role for Rad53 was to ensure replication forks successfully traversed *CEN*s in HU, allowing replicating chromosomes to achieve amphitelic attachment (Bachant *et al.*, 2005). Four observations supported this model. First, mutations affecting the essential K proteins Ndc10, Mif2, and Ndc80 and Ask1—components of K subcomplexes linking *CEN* chromatin to the MT interface—all induced spindle extension in HU (see also Ma *et al.*, 2007; Liu *et al.*, 2008). Second, dicentric chromosomes rescued *rad53* spindle extension. Third, Ipl1/Aurora B, which is required to efficiently orient Ks to both spindle poles (Tanaka *et al.*, 2002), displayed HU spindle extension. Fourth, minichromosomes where *CEN*s are juxtaposed to *ORI*s blocked *rad53* spindle extension in HU. Our interpretation was that these minichromosomes allowed a threshold number of *CEN*s to be duplicated prior to nucleotide exhaustion, compensating for loss of Rad53.

A prediction stemming from the above observations is that Rad53 should prevent HU spindle extension through the same checkpoint substrates as DNA replication fork control. Here we provide evidence this is true, as loss of Rad53 regulation of *ORI* firing and RNR is sufficient to induce spindle extension. HU-treated *rad53* mutants show a loss of both *CEN* DNA and K integrity, providing an explanation for how DNA replication and spindle control are integrated within the checkpoint. A second issue concerns whether *CEN* duplication is required to offset S phase spindle extension. Remarkably, we find *CEN* duplication can lag bipolar spindle assembly, raising the question as to why K attachments are required to stabilize spindle length during an extended S phase. We address this by proposing an S phase spindle structure in which monotelic attachments between immobilized S phase *CEN*s and the spindle generate an inward-acting force that offsets spindle extension.

RESULTS

Rad53 regulation of ORI firing is coupled to spindle extension in HU

As set out in the *Introduction*, we initially hypothesized that failure of forks to traverse *CEN*s in HU was the proximal cause of *rad53* spindle extension. Interestingly, an inability to duplicate *CEN*s is also thought to be responsible for the reductional anaphase phenotype of replication initiation-defective *cdc6*, *cdc7*, and *dbf4* mutant strains (Piatti *et al.*, 1995; Warsi *et al.*, 2008). Dbf4 is a regulatory subunit for the Cdc7 kinase (Dbf4-dependent kinase, DDK), an essential and limiting activator of *ORI* firing (Jackson *et al.*, 1993; Bousset and Diffley, 1998; Mantiero *et al.*, 2011); Cdc6 is a replication initiation protein that localizes to presumptive *ORI*s as part of the prereplication complex (pre-RC; Cocker *et al.*, 1996). Notably, the role of Rad53 in delaying *ORI* firing in HU (Rad53-checked *ORI*s) has been shown to be important in stabilizing replication forks from early firing (unchecked) *ORI*s, presumably by minimizing competition between forks for limiting factors such as dNTPs (Poli *et al.*, 2012; Zhong *et al.*, 2013; Morafraile *et al.*, 2015). We therefore considered whether the inability to fire *ORI*s in *ddk* mutants and unrestrained *ORI* firing in HU-treated *rad53* mutants might lead to spindle extension for the same reason—namely, a failure in *CEN* duplication. An experimental approach to test this was suggested by the observation that *cdc7-1* temperature-sensitive mutants delay firing of some Rad53-checked *ORI*s when released from a HU block at a nonpermissive temperature (Boussett and Diffley, 1998). On the basis of these considerations, we conducted a series of temperature shift experiments in HU using conditional alleles affecting the DDK in combination with *rad53*. The rationale was that, by shifting *rad53 ddk* mutants to a *ddk* nonpermissive temperature at particular windows in S-phase, it might be possible to reduce *ORI* firing, including

firing of some *ORI*s that would otherwise be activated due to loss of Rad53. This could, in turn, potentially mitigate fork destabilization, allowing *CEN*s to be duplicated and suppressing spindle extension in *ddk rad53* double mutants. Accordingly, *dbf4-1 mec1-21*, *cdc7-1 rad53-21*, and *dbf4-1 rad53-21* double mutants were released from G_1 into media containing 200 mM HU at a permissive temperature of 25°C. Starting at 15 min postrelease, cultures were shifted to a nonpermissive temperature at different times to inactivate the DDK. We observed there was a window 30–55 min postrelease where shifting *mec1 ddk* and *rad53 ddk* mutants resulted in a two- to threefold reduction in cells displaying spindle extension (Figure 1, A–C). One explanation for this window is that few *ORI*s fire in *mec1 ddk* and *rad53 ddk* mutants when the DDK is inactivated before 30 min, leading to a reductional anaphase. Inactivating the DDK after 55 min, on the other hand, is too late to prevent *ORI* firing, leading to spindle extension in a manner similar to *mec1* and *rad53* controls. Extending these results, we found that overproduction of Dbf4, which advances *ORI* firing, including *ORI*s that are normally checked in HU (Mantiero *et al.*, 2011; Tanaka *et al.*, 2011), was sufficient to force HU spindle extension in checkpoint-proficient cells. Cooverproduction of Rad53, which binds to and phosphorylates Dbf4 in HU (Duncker *et al.*, 2002; Chen *et al.*, 2013; Matthews *et al.*, 2014; Almawi *et al.*, 2016), rescued this defect (Figure 1D).

To clarify the epistasis between *rad53* and the *dbf4* mutations with respect to HU spindle extension, we screened a mutagenized plasmid library for p*dbf4* ("p" designates plasmid-based expression) clones that partially suppressed the temperature sensitivity of *dbf4-1* and did not exhibit a reductional anaphase. Our presumption was such clones would encode hypomorphic p*dbf4* alleles that would reduce *ORI* firing overall, while still supporting sufficient firing of *CEN* flanking *ORI*s to replicate *CEN*s. Three p*dbf4* clones that satisfied these criteria were obtained (Khalil *et al.*, 2007). All three harbored nonsense or missense mutations affecting the C-terminus of Dbf4 (collectively referred to as p*dbf4-C*; Figure 2A). The Dbf4 C-terminus contains a C2H2 Zn^{2+} finger domain embedded within a 41 amino acid region known as motif-C (Masai and Arai, 2000). Motif-C forms one of two Dbf4 contact surfaces with Cdc7, and, in yeast, it has been shown that the Zn^{2+} finger plays a nonessential role in stimulating DDK activity (Harkins *et al.*, 2009; Jones *et al.*, 2010; Hughes *et al.*, 2012). We therefore constructed an additional allele, *dbf4-zn*, which deletes Dbf4 residues 660–688 involved in forming the Zn^{2+} finger (Figure 2A). Analysis of these *dbf4* alleles in the absence of HU indicated, first, similar to p*dbf4-C*, p*dbf4-zn* only partially complemented *dbf4-1* when expressed from a low copy plasmid (Figure 2B). Second, in agreement with previous work (Harkins *et al.*, 2009; Jones *et al.*, 2010), *dbf4-zn* exhibited a temperature-sensitive growth defect and slow progression through S phase when integrated at the endogenous locus (Figures 2D and 3A). Third, strains expressing integrated *dbf4-zn* arrested as budded cells with short preanaphase spindles at a nonpermissive temperature of 37°C (Figure 3B). Fourth, as with *dbf4-1* (Warsi *et al.*, 2008), *dbf4-zn* cell cycle arrest was dependent on the spindle assembly checkpoint (SAC; Figure 3C). Fifth, a surprising finding was that p*dbf4-C* or p*dbf4-zn* expressed over a deletion of *DBF4* grew at temperatures up to 37°C (Figure 2C). Thus, while *dbf4-1* cells transformed with p*dbf4-C* or p*dbf4-zn* were temperature sensitive, *dbf4-Δ* cells transformed with p*dbf4-C* or p*dbf4-zn* were not. It is likely that *dbf4-1* has a partial dominant negative activity toward p*dbf4-C* and p*dbf4-zn* and that the low-copy plasmids used in these experiments lead to increased p*dbf4* expression compared with the endogenous locus.

Using p*dbf4-C* and p*dbf4-zn*, we reexamined *ddk* suppression of *rad53* spindle extension in HU without having to circumvent the reductional anaphase phenotype associated with *dbf4-1*. *rad53* can display synthetic lethality with *ddk* mutations (Dohrmann and Sclafani, 2006), and spores combining *rad53-21* with integrated *dbf4-zn* were inviable (unpublished data). However, we readily isolated *rad53-21 dbf4-Δ* segregants containing p*dbf4-C* or p*dbf4-zn*; such transformants were therefore used in subsequent experiments. We found that our three p*dbf4-C* alleles, as well as p*dbf4-zn*, provided a robust block to *rad53* spindle extension in HU, lowering the percentage of cells with spindles ≥3 μm—our threshold for an extended spindle (Bachant *et al.*, 2005)—from ~50% in *rad53-21 dbf4-Δ/pDBF4* strains to 4–11% in *rad53-21 dbf4-Δ/pdbf4-C* and *rad53-21 dbf4-Δ/pdbf4-zn* double mutants (Figure 4, A and B). Suppression of spindle extension was not accompanied by amelioration of *rad53-21* HU sensitivity (Figure 4C), or HU recovery (Figure 4D). The essential role of the DDK in *ORI* firing is to phosphorylate MCM proteins to assemble the CMG replicative helicase (Hardy *et al.*, 1997; Sheu and Stillman, 2010). If p*dbf4* alleles suppress spindle extension by reducing MCM activity, *mcm* mutations should behave similarly. This proved to be the case, as the percentage of cells with spindles ≥3 μm was reduced from 65% in *rad53-21* to 5% in HU-treated *mcm2-1 rad53-21*, *mcm3-1 rad53-21*, and *mcm5-1 rad53-21* mutants (Figure 4A).

Dbf4, Sld3 and Dun1 are Rad53 substrates in blocking spindle extension

The results presented so far suggest that Rad53 delay of *ORI* firing in HU might be important in restraining spindle extension. This delay is mediated through Rad53 inhibitory phosphorylation of Dbf4 and another CMG activator, Sld3. A *dbf4-m25 sld3-38A* mutant that is resistant to Rad53 phosphorylation exhibits firing of checked *ORI*s even though Rad53 is activated normally (Lopez-Mosqueda *et al.*, 2010; Zegerman and Diffley, 2010). In three experiments we found that, on average, ~50% of *dbf4-m25 sld3-38A* cells (56%, 52%, 42%) released into HU displayed spindles ≥3 um compared with 63% for *rad53-21* controls (67%, 67%, 54%; Figure 5, A and B). While the frequency of *dbf4-m25 sld3-38A* spindle extension is similar to *rad53-21*, the average length of *dbf4-m25 sld3-38A* spindles was slightly, but significantly, reduced (mean 3.0 μm compared with 3.5 μm for *rad53-21*, $p < 0.001$), and the fraction of spindles >4 μm was noticeably diminished (Supplemental Figure S1). Importantly, Dun1 is another Rad53 substrate that contributes to fork stability in HU by expanding dNTP pools (Poli *et al.*, 2012; Morafraile *et al.*, 2015). We therefore examined the effect of ablating both Dun1 and the block to *ORI* firing (see Figure 10A, red X's on pathways 1 and 2, later in this article). An average of 72% of *dun1-Δ dbf4-m25 sld3-38A* triple mutants (79%, 71%, 66%) exhibited spindle extension in HU (Figure 5, A and B), with a distribution of spindle lengths that was largely similar to *rad53-21* (Supplemental Figure S1). Thus, short-circuiting Rad53 regulation of Dbf4, Sld3 and Dun1 synergizes to phenocopy *rad53* spindle extension in HU. Consistent with previous observations indicating DNA replication control is an essential function of the S phase checkpoint (Desany *et al.*, 1998), *dun1-Δ dbf4-m25 sld3-38A* mutants also exhibited a synergistic increase in HU sensitivity approaching that of *rad53-21* (Figure 5C).

dbf4-zn reduces ORI firing in rad53 mutants

Our initial rationale for how spindle extension might be suppressed in HU-treated *dbf4-zn rad53* double mutants made two testable predictions. First, we predicted *dbf4-zn rad53* double mutants should exhibit reduced utilization of some, or (given the hypomorphic

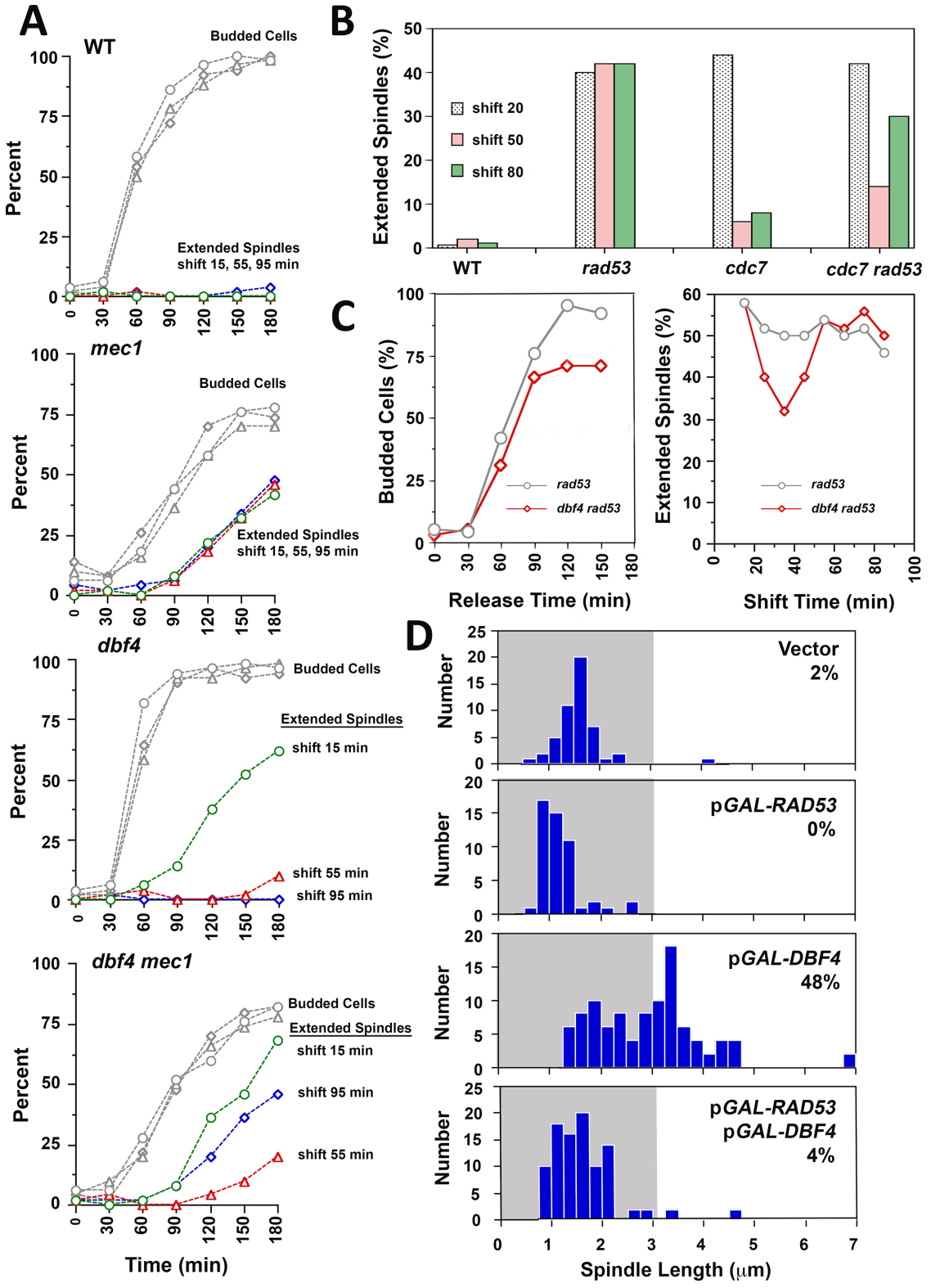

FIGURE 1: DDK temperature-sensitive alleles reduce spindle extension in S phase checkpoint mutants. (A) WT (Y300), *mec1-21* (AY201), *dbf4-1* (JBY999), and *mec1-21 dbf4-1* (JBY927) strains were released from G_1 at 25°C in 200 mM HU media. At 15, 55, or 95 min after G_1 release, cultures were shifted to a nonpermissive temperature of 34°C. At times indicated on the *x*-axis, aliquots were processed for α-tubulin immunofluorescence and DAPI staining. Spindle extension was reduced in *mec1-21 dbf4-1* cells shifted at 55 min. (B) WT (Y300), *rad53-21* (Y301), *cdc7-1* (DES956), and *rad53-21 cdc7-1* (DES960) were released into 200 mM HU media as in A and were shifted to 35°C at 20, 50, and 80 min. After a total of 180 min following G_1 release, cells were processed for α-tubulin immunofluorescence and DAPI. As with *mec1-21 dbf4-1* cells, *rad53-21 cdc7-1* cells displayed reduced spindle extension when shifted at 50 min. (C) To more closely bracket the window for suppression of spindle extension, *rad53-21* (Y301) and *rad53-21 dbf4-1* (JBY1002) strains

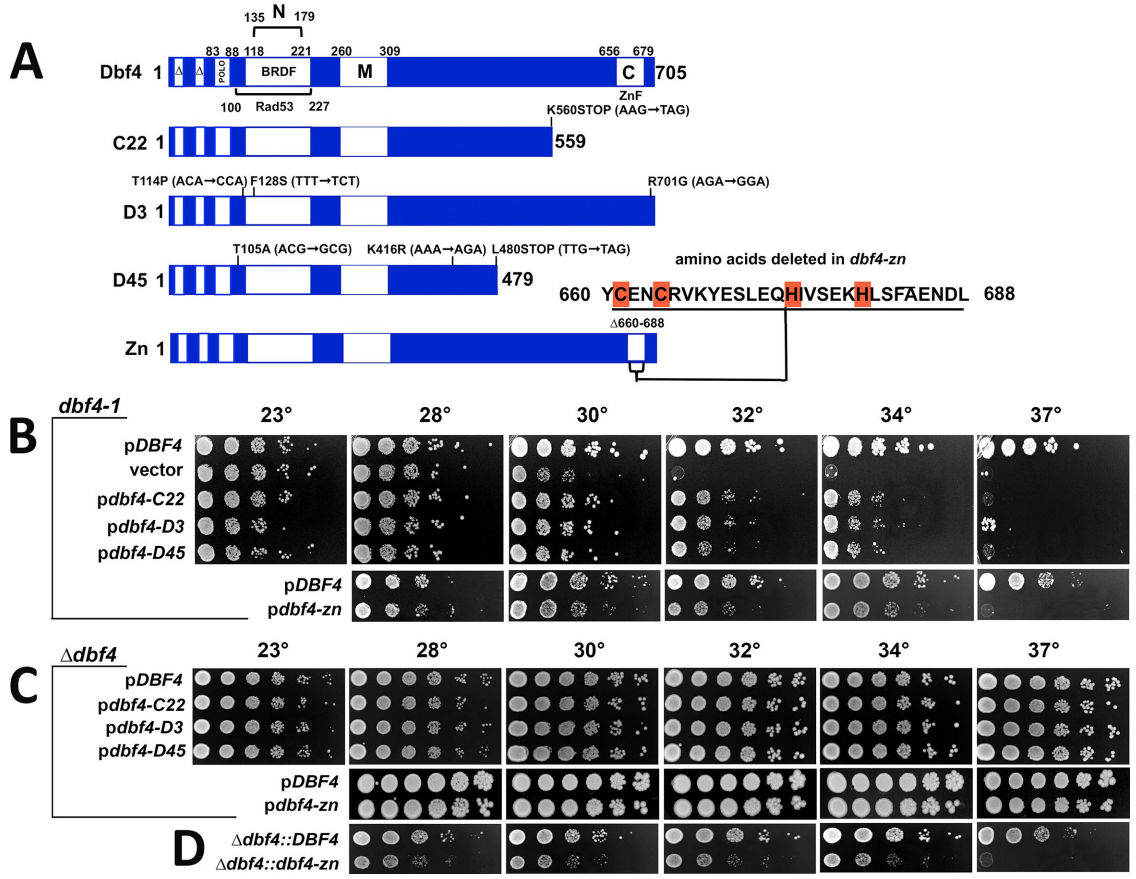

FIGURE 2: Characterization of *dbf4-C* and *dbf4-zn*. Experiments in this figure are without HU treatment. (A) Dbf4 domains and mutant alleles. C22, D3, and D45 are PCR mutagenized alleles, while *dbf4-zn* was constructed using recombinant techniques. Base pair changes that alter amino acid coding in *dbf4-C* alleles are indicated; Zn^{2+} finger amino acids deleted in *dbf4-zn* are also shown. The diagram also illustrates amino acid boundaries for domains involved in cell cycle proteolysis (Δ); Cdc5 (Polo) and Rad53 binding; motifs N, M, and C; and the BRCT-related BFDF domain. (B) Complementation of *dbf4-1*; 10-fold serial dilutions of a *dbf4-1* strain (JBY997) transformed with low copy p*CEN ARS DBF4* (JJY059; JJY164), vector (JJY016), p*dbf4-C22* (JJY017), p*dbf4-D3* (JJY060), p*dbf4-D45* (JJY061), and p*dbf4-zn* (JJY165) plasmids were stamped onto selective media at indicated temperatures. Whereas *DBF4* complements *dbf4-1* to 37°C, *dbf4-C* and *dbf4-zn* alleles partially complement to 34°C. (C) Complementation of *dbf4-*Δ. A *dbf4-*Δ strain harboring p*URA3 DBF4* was transformed with p*CEN ARS DBF4* (JJY037, JJY166), p*dbf4-C22* (JJY032), p*dbf4-D3* (JJY033), p*dbf4-D45* (JJY044), and p*dbf4-zn* (JJY167). The transformants were cured of the covering *DBF4 URA3* plasmid on 5′-FOA; 10-fold serial dilutions were stamped onto selective media at indicated temperatures. In this case, low copy *dbf4-C* and *dbf4-zn* plasmids complement *dbf4-*Δ growth to 37°C. (D) Integrated *dbf4-zn*. Constructs expressing *DBF4* (JJY046) or *dbf4-zn* (JJY076) were integrated immediately upstream of a precise deletion of the *DBF4* open reading frame; 10-fold serial dilutions were incubated at indicated temperatures revealing a *dbf4-zn* temperature sensitive growth phenotype.

nature of *dbf4-zn*) perhaps all, *ORI*s in HU compared with *rad53* single mutants. Second, reduced *ORI* utilization should correspond with improved duplication of *CEN*s. To examine these predictions, ssDNA hybridization to genome microarrays was used to analyze *ORI* firing in HU (Feng *et al.*, 2007). In a first experiment, *dbf4-*Δ cells harboring p*DBF4* or p*dbf4-zn* were released from G_1 into 200 mM HU at 30°C. After 60 min, ssDNA was isolated and processed for replication profiling. A total of 177 *ORI*s activated in *dbf4-*Δ/p*DBF4* and *dbf4-*Δ/p*dbf4-zn* strains was detected (Figure 6A and Supplemental Figure S2). To quantify the effect of p*dbf4-zn* on *ORI*

were released from G_1 into 200 mM HU at 25°C and then split into parallel cultures, which were then shifted to 34°C at the indicated times on the *x*-axis of the right-hand graph (shift time). Aliquots were maintained at 25°C to monitor cell budding (left graph). Spindle extension was evaluated in temperature-shifted samples at 150 min post-G_1 release using DAPI and α-tubulin immunofluorescence (right graph). Maximal suppression of spindle extension was observed when *rad53-21 dbf4-1* cells were shifted at 40 min, corresponding with bud emergence and S phase entry. (D) *SPC42-GFP* cells (JBY1129) were transformed with vector (JBY1285), a low copy plasmid expressing *RAD53* under control of the inducible *GAL* promoter (p*CEN HIS3 GAL-RAD53*, JBY1286), a high copy p*GAL-DBF4* plasmid (p2μm *URA3 GAL-DBF4*; JBY1287), or cotransformed with both plasmids (JBY1288). Transformants were arrested in G_1 for 3.5 h in galactose media (YPGAL) to induce *RAD53* and/or *DBF4*. Cells were then released into YPGAL containing 200 mM HU. After 3.5 h, spindle extension was evaluated using Spc42-GFP.

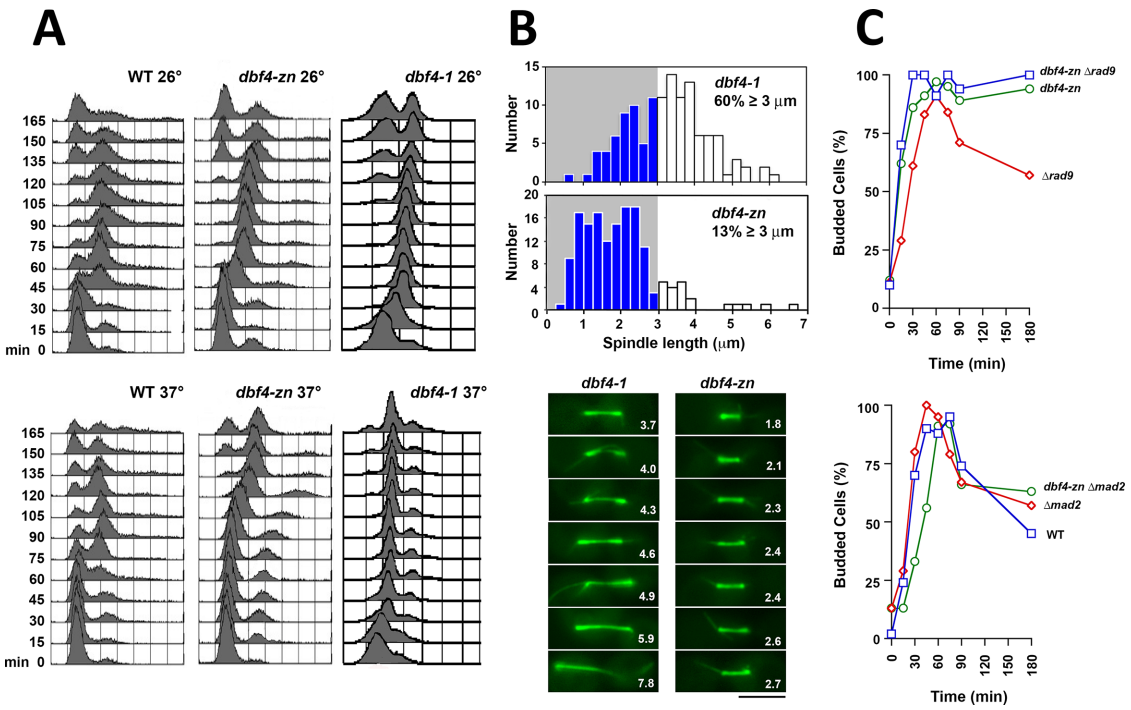

FIGURE 3: *dbf4-zn* does not undergo a reductional anaphase. Experiments in this figure are without HU treatment. (A) FACs. WT (CRY1), *dbf4-1* (JBY999), or *dbf4-zn* expressed from the native locus (JJY076) strains were arrested in G_1, released at 26°C or 37°C, and analyzed by FACs. *dbf4-zn* shows an ~15 min S phase delay compared with WT at 26°C and an ~45–60 min delay at 37°C. (B) Top graphs: a *dbf4-1 SPC42-GFP* strain (JBY1392) and a strain expressing *SPC42-GFP* and integrated *dbf4-zn* (JJY045) were released from G_1 at 37°C. After 2 h, spindle length distributions were determined using Spc42-GFP. Bottom micrographs: *dbf4-1* (JBY2323) and integrated *dbf4-zn* (JBY2324) cells expressing *GFP-TUB1* were released from G_1 at 37°C. After 2 h spindles were visualized at 37°C. Numbers, spindle length in μm; bar, 4 μm. Whereas *dbf4-1* exhibits reductional anaphase spindle extension, *dbf4-zn* arrests with normal length preanaphase spindles. (C) The *dbf4-zn* cell cycle arrest. Top graph: *rad9*-Δ (JBY186), integrated *dbf4-zn* (JJY076) and integrated *dbf4-zn rad9*-Δ (JJY080) double mutants were released from G_1 at 37°C, and budding was used to evaluate cell cycle progression. Bottom graph: WT (CRY1), *mad2*-Δ (JBY546), and integrated *dbf4-zn mad2*-Δ (JJY102) strains were analyzed similarly. As with *dbf4-1*, *dbf4-zn* cell cycle arrest is dependent on Mad2 but not Rad9.

utilization in HU, the area under each ssDNA *ORI* curve (*ORI* AUC) in the data sets was used to calculate an *ORI* AUC ratio comparing *dbf4-Δ/pdbf4-zn* to *dbf4-Δ/pDBF4*. The mean p*dbf4-zn*/p*DBF4* *ORI* AUC ratio for all 177 *ORI*s was 0.74, an ~25% reduction (Supplemental Figure S4A). Strikingly, many *ORI*s in the vicinity of *CEN*s displayed a substantially stronger reduction in HU (Figure 6, A and B; Supplemental Figures S2 and S4A). The set of 32 *CEN*-flanking *ORI*s (Supplemental Figure S4B) showed the greatest down-regulation, with a mean p*dbf4-zn*/p*DBF4* *ORI* AUC ratio of 0.36 (red in Figure 6B, Supplemental Figure S4A; Supplemental Tables S1 and S2, $p < 0.0001$). Not all *CEN*-flanking *ORI*s were affected equivalently (Supplemental Table S2), however, and some *ORI*s that did not immediately flank a *CEN* were also reduced (Supplemental Figure S2 and Supplemental Table S3). As a second treatment, we queried the data sets to detect *ORI* peaks whose amplitudes were altered by three standard deviations from the median difference between HU-treated *dbf4-Δ/pdbf4-zn* and *dbf4-Δ/pDBF4* (Supplemental Table S3). Thirty-two strongly reduced *ORI*s were identified, including 20 *CEN* flanking *ORI*s. Interesting, 19 differentially up-regulated *ORI*s were also observed (Supplemental Table S3); these tended to be less efficiently utilized *ORI*s (Supplemental Figure S4A). To visualize a spatial basis for these patterns, positions for the 32 down-regulated *ORI*s and 19 up-regulated *ORI*s were mapped onto a spatial model of chromosome organization in the yeast nucleus (Duan *et al.*, 2010). Down-regulated *ORI*s (blue) were closely associated with the *CEN* cluster (red), while up-regulated *ORI*s (green) tended to reside just beyond the periphery of the *CEN* cluster (Figure 6C).

We next proceeded to examine ssDNA replication profiles for 403 *ORI*s detected in HU-treated *rad53-21 dbf4-Δ* mutants transformed with p*DBF4*, p*dbf4-zn*, or p*dbf4-D3* (a p*dbf4-C* allele harboring R701G, Figure 2A). Utilization of all 403 *ORI*s was substantially reduced in *rad53-21 dbf4-Δ/pdbf4-zn* compared with *rad53-21 dbf4-Δ/pDBF4*, with a mean *ORI* AUC ratio of 0.26 (Figure 6, A and B; Supplemental Figures S2, S3, and S4A). The set of 32 *CEN*-flanking *ORI*s, however, still showed a preferential reduction (*ORI* AUC ratio 0.15, red in Figure 6B and Supplemental Figure S4A, $p < 0.0001$). The *rad53-21 dbf4-Δ/pdbf4-D3* HU data set trended similarly, although *ORI* diminishment was not as pronounced, with an *ORI* AUC ratio of 0.72 for all 403 ORIs and 0.61 for *CEN*-flanking *ORI*s (Figure 6, A and B; Supplemental Figures S3 and S4A, $p < 0.0001$ for both comparisons). Overall, these results reveal that the Zn^{2+} finger of Dbf4 makes a complex contribution to *ORI* firing in HU. When the S phase checkpoint is active, this contribution is strongly manifested in the vicinity of *CEN*s. When the S phase checkpoint is inactive, however, global *ORI* firing become more reliant on the Zn^{2+} finger. In terms of our first prediction, the HU replication profiles of *rad53-21 dbf4-Δ/pdbf4-zn* mutants clearly show reduced *ORI* utilization in HU compared with *rad53-21 dbf4-Δ/pDBF4*-consistent with our expectations. With respect to our second prediction, however,

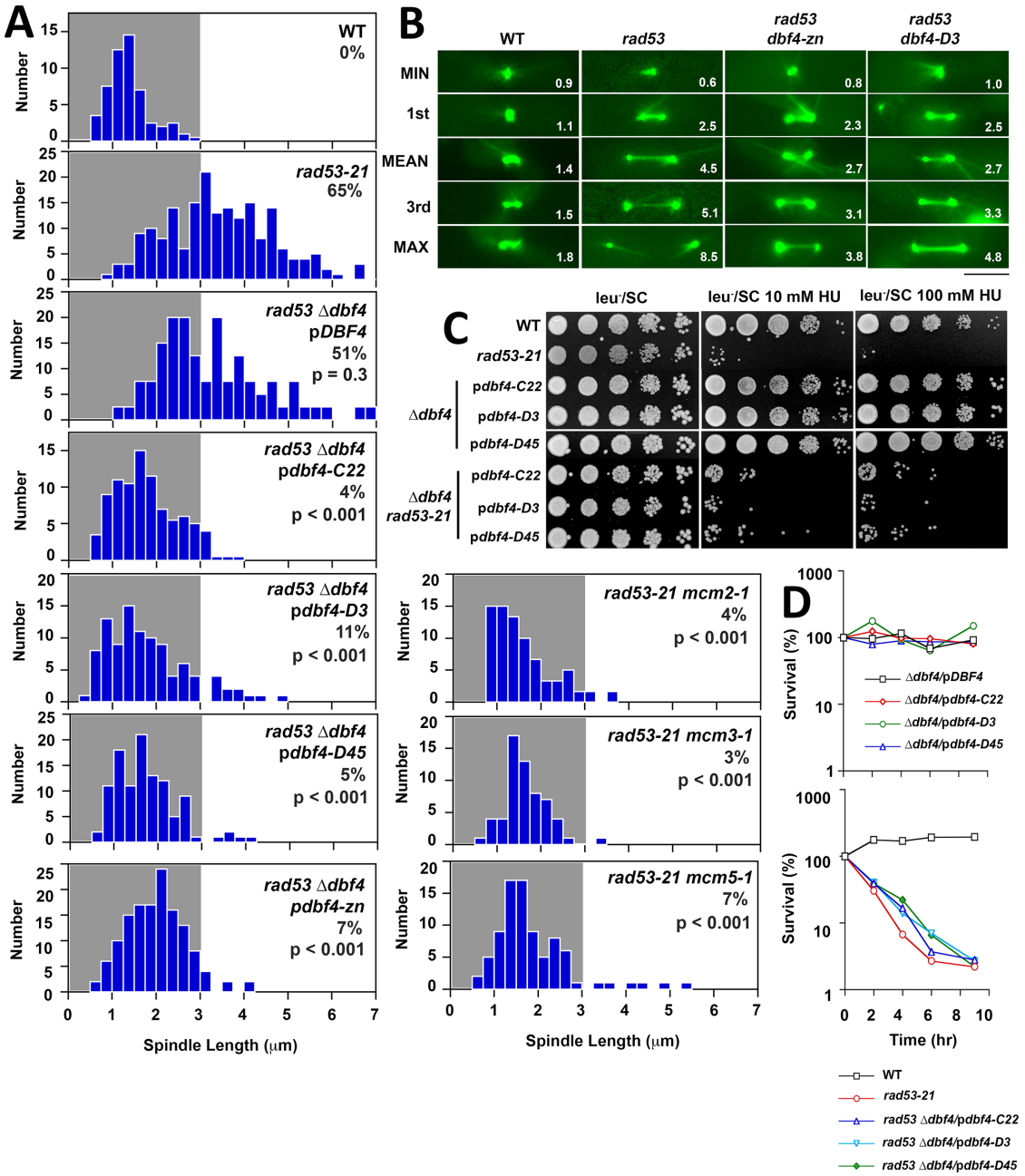

FIGURE 4: p*dbf4 C*, p*dbf4-zn* and *mcm* alleles suppress *rad53* spindle extension in HU. (A) WT (JBY1129), *rad53-21* (JBY1274), *rad53-21 dbf4-Δ*/p*DBF4* (JJY184), *rad53-21 dbf4-Δ*/p*dbf4-C22* (JJY028), *rad53-21 dbf4-Δ*/p*dbf4-D3* (JJY029), *rad53-21 dbf4-Δ*/p*dbf4-D45* (JJY030), *rad53-21 dbf4-Δ*/p*dbf4-zn* (JJY182), *rad53-21 mcm2-1* (JJY112), *rad53-21 mcm3-1* (JJY117), and *rad53-21 mcm5-1* (JJY120) strains, all harboring *SPC42-GFP*, were released from G_1 into 200 mM HU at 30°C. After 90 min spindle lengths were measured in fixed cells. Percentages of cells with spindles ≥3 μm are displayed, along with the results of two-tailed *t* tests comparing each mutant to the *rad53-21* distribution. (B) WT (JBY1129), *rad53-21* (JBY1274), *rad53-21 dbf4-Δ*/p*dbf4-zn* (*rad53 dbf4-zn* on the figure; JJY182), and *rad53-21 dbf4-Δ*/p*dbf4-D3* (*rad53 dbf4-D3* on the figure; JJY029) strains were transformed with p*GFP-TUB1* to visualize MTs. Cells were released from G_1 into 200 mM HU at 30°C. Starting at 90 min, spindles were imaged and measured (values at the bottom right of each panel) in 50 live cells. Spindles corresponding to minimum, maximum, mean, first, and third quadrant measurements are shown. Bar, 4 μm. (C) Tenfold serial dilutions of WT (JBY1129), *rad53-21* (JBY1274), *dbf4-Δ*/p*DBF4* (JJY037), *dbf4-Δ*/p*dbf4-C22* (JJY032), *dbf4-Δ*/p*dbf4-D3* (JJY033), and *dbf4-Δ*/p*dbf4-D45* (JJY044) strains, along with *rad53-21 dbf4-Δ* transformants described in A were stamped on indicated media at 30°C to evaluate HU sensitivity. (D) Asynchronous cultures of all the strains described in C were shifted into media containing 200 mM HU at 30°C. At the indicated times, plating efficiency was determined to evaluate HU recovery.

the pattern of *ORI* firing does not necessarily support the idea that *CEN* duplication is required for suppression of spindle extension in HU. This is because the exact population of *ORI*s whose firing would be expected to give rise to *CEN* duplication was the most strongly reduced in *rad53-21 dbf4-Δ*/p*dbf4-zn*. In fact, a different interpretation of the *rad53-21 dbf4-Δ*/p*dbf4-zn* data set is that preventing,

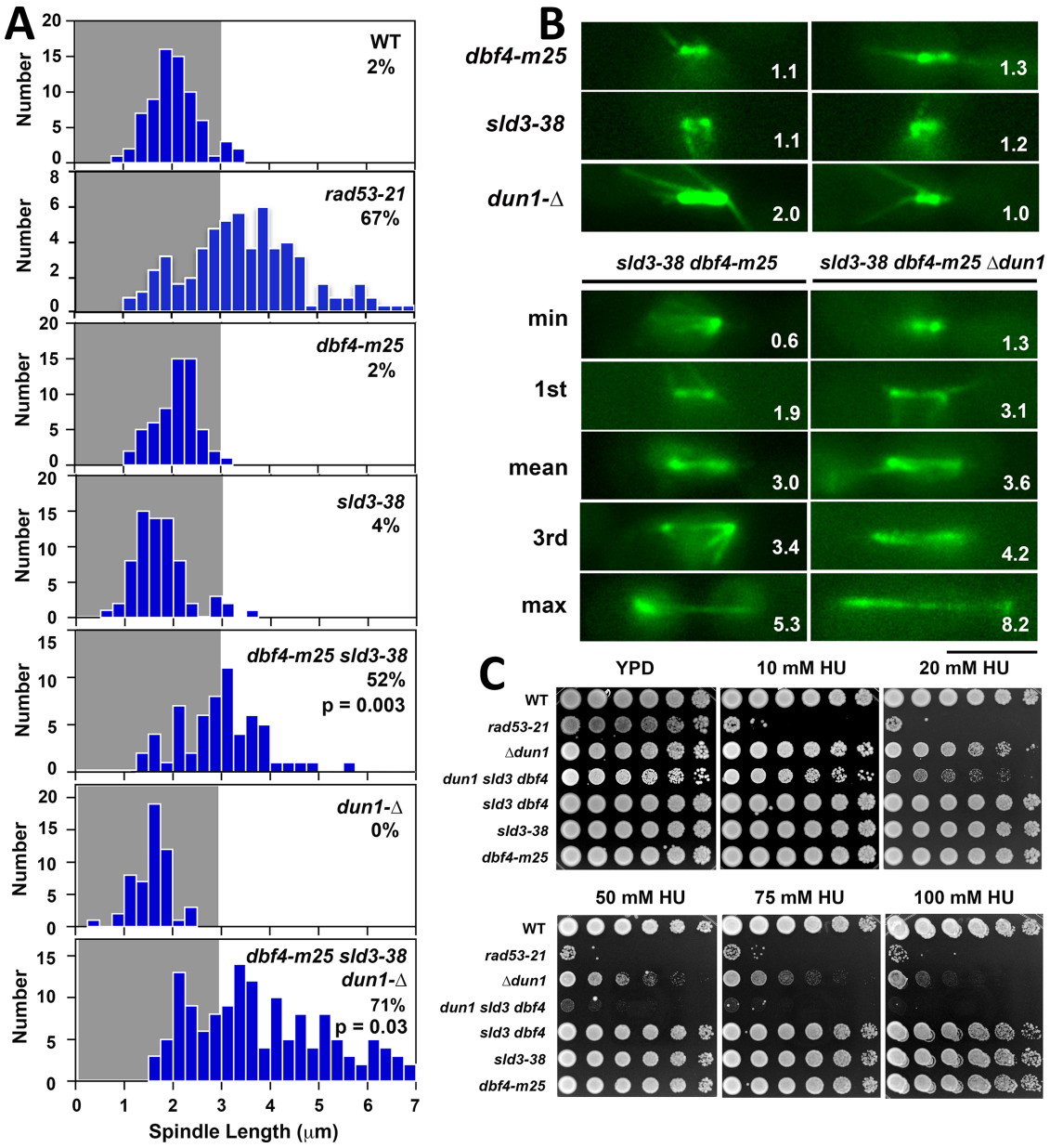

FIGURE 5: Dbf4 and Sld3 are Rad53 substrates controlling the block to spindle extension. (A) WT (CRY1), *rad53-21* (Y301), *dbf4-m25* (YJLO157), *sld3-38A* (YJLO156), *dbf4-m25 sld3-38A* (YJLO155, JBY2334), *dun1*-Δ (MY26), and *dbf4-m25 sld3-38A dun1*-Δ (JJY141, JJY144) strains were arrested in G_1 and released into 200 mM HU at 30°C. After 90 min, samples were processed for α-tubulin immunofluorescence, and spindle lengths were measured. The percentage of cells with spindles ≥3 μm is shown, along with *p* values (two-tailed *t* test) comparing the *sld3-38A dbf4-m25* and *sld3-38A dbf4-m25 dun1*-Δ distributions to *rad53-21*. (B) Strains in A were transformed with p*GFP-TUB1*, arrested in G_1, released into 200 mM HU at 30°C, and spindles were imaged and measured in live cells. Representative spindles are shown for *dbf4-m25*, *sld3-38A*, and *dun1*-Δ single mutants, along with spindles corresponding to minimum, maximum, mean, first, and third quadrant measurements from the *sld3-38A dbf4-m25* and *sld3-38A dbf4-m25 dun1*-Δ populations. Numbers in panels, spindle length in μm; bar, 4 μm. (C) Tenfold serial dilutions of strains in A were stamped onto indicated media to evaluate HU sensitivity.

rather than promoting, replication in the vicinity of *CEN*s might correspond with rescue of spindle extension in HU-treated *rad53-21 dbf4-Δ/pdbf4-zn* mutants.

In light of the realization that avoiding replication fork destabilization in proximity to *CEN*s might underlie suppression of spindle extension in HU-treated *rad53* mutants, several additional analyses were performed. First, using the 16 *ORI*s closest to each *CEN* (Supplemental Figure S4B; Supplemental Tables S1 and S2), we generated composite HU replication profiles for *dbf4-Δ/pDBF4* cells and *rad53-21 dbf4-Δ/pDBF4* mutants (Figure 7A). The *dbf4-Δ/pDBF4* cells display a characteristic split peak profile indicative of bidirectional replication fork movement. The *rad53-21 dbf4-Δ/pDBF4* mutants, in contrast, tend to display a single ssDNA peak whose maximum amplitude is centered over the *ORI*, reflecting accumulation of aberrant ssDNA. ssDNA values for CDEI, II, and III *CEN* DNA elements from the *dbf4-Δ/pDBF4*, *dbf4-Δ/pdbf4-zn*, *rad53-21*

dbf4-Δ/pDBF4, and *rad53-21 dbf4-Δ/pdbf4-zn* data sets were superimposed on these HU replication composites. The *rad53-21 dbf4-Δ/pDBF4* showed a comparative increase in ssDNA at *CEN*s 2, 3, 9, and 16, the four closest *CEN*s to an *ORI* (Figure 7A). In contrast, only baseline levels of *CEN* ssDNA were observed in *dbf4-Δ/pdbf4-zn* and *rad53-21 dbf4-Δ/pdbf4-zn*. Second, we used the *dbf4-Δ/pDBF4* and *dbf4-Δ/pdbf4-zn* composite profiles to perform a statistical analysis of *CEN* duplication in HU (Supplemental Results). We found that between 60 and 90 min, ≥98% of HU-treated *dbf4-Δ/pDBF4* cells are predicted to have duplicated a minimum of 6–8 *CEN*s (Figure 7B, Supplemental Figure S5B, and Supplemental Tables S4 and S5). In contrast, during the same period ~10% of *dbf4-Δ/pdbf4-zn* cells have not duplicated any *CEN*. Third, *ctf19-Δ* strains defective for the Ctf19/COMA K complex fail to recruit the DDK to Ks and, like *dbf4-Δ/pdbf4-zn*, exhibit reduced firing of *CEN*-proximal *ORI*s (Natsume *et al.*, 2013; Hinshaw *et al.*, 2017). We therefore tested whether loss of Ctf19 behaved similarly to p*dbf4-zn* in suppressing *rad53* spindle extension in HU. Unlike our previous results with strains defective for essential K proteins (Bachant *et al.*, 2005), *ctf19-Δ* and *mcm21-Δ* mutants arrested with short spindles in HU, and spindle extension in *rad53-21 ctf19-Δ* and *rad53-21 mcm21-Δ* strains was reduced to 11% ($p < 0.001$) and 12% ($p < 0.001$) compared with 48% for *rad53-21* controls (Figure 6D).

Exo1 is a determinant of CEN/K integrity in HU-treated *rad53* mutants

The exonuclease Exo1 is responsible for much of the aberrant ssDNA that is generated at replication forks in HU-treated *rad53* mutants (Cotta-Ramusino *et al.*, 2005; Feng *et al.*, 2006). During this study, we noticed GFP chromosome tags in the vicinity of *CEN*s often exhibited reduced fluorescence in *rad53* mutants exposed to HU (Figure 8B). To determine whether this loss of signal might be a result of Exo1 activity, LacO arrays were integrated adjacent to the *CEN* on chromosomes 2 (*CEN2-GFP*), 9 (*CEN9-GFP*), and 10 (*CEN10-GFP*) and visualized using LacI-GFP (Supplemental Figures S6 and S7). We also targeted LacO arrays to regions on chromosomes 9 and 10 ~20 kbp distant from *ORI*s in wild type (WT) and *rad53* cells (*LATE9-GFP* and *LATE10-GFP*; Supplemental Figures S6 and S7); these regions are unlikely to be duplicated during the initial phase of HU treatment. WT, *rad53-21*, and *rad53-21 exo1-Δ* strains harboring *CEN-GFP* and *LATE-GFP* were released into HU, or into media containing nocodazole (NZ). For all tags, we observed the anticipated increase in fluorescence in NZ, reflecting duplication of the tags (Figure 8C). In contrast, for WT cells, median tag intensity only increased slightly in HU. In HU-treated *rad53* cells, *CEN2-GFP* ($p < 0.001$), *CEN9-GFP* ($p < 0.001$), and *CEN10-GFP* ($p = 0.02$) all showed significant decreases in fluorescence (Figure 8C and Supplemental Figure S8A). Such a decrease was not observed in *rad53 exo1-Δ CEN9-GFP*, *rad53 exo1-Δ CEN10-GFP*, *rad53 LATE9-GFP*, or *rad53 LATE10-GFP* strains. Thus, reduced tag intensity in HU-treated *rad53* cells is influenced by both *Exo*1 and tag distance from an *ORI*. To examine whether *rad53* mutants might also display an *Exo*1-mediated disruption of K integrity in HU, WT, *rad53-21*, and *rad53-21 exo1-Δ* strains harboring the K protein Mtw1-GFP were released into media containing both HU and NZ. Bud circumference was measured as a proxy for elapsed time in S phase. Whereas HU-treated WT cells showed a gradual increase in Mtw1-GFP signal as bud size increased, Mtw1-GFP intensity decreased in *rad53* cells (Figure 8D, $p < 0.001$). This decrease was partially ameliorated in *rad53 exo1-Δ*, which showed an intermediate distribution of Mtw1-GFP intensities.

We then examined spindle length in HU-treated WT, *exo1-Δ*, *rad53-21*, and *rad53-21 exo1-Δ* strains, again using bud circumference as a metric for elapsed time in S phase. For HU-treated *rad53* mutants, spindle extension is observed shortly after spindle poles separate (Bachant *et al.*, 2005). Consistent with this, 42% of *rad53* cells with a bud circumference of ≤15 μm (small- to medium-budded cells) exhibited extended spindles (red diamonds, Figure 8E), and 40% of cells with buds >15 μm (medium- to large-budded cells) showed extended spindles (orange diamonds). In comparison, only 7% of small- to medium-budded *rad53 exo1-Δ* exhibited spindle extension (sixfold decrease, $p < 0.001$), while 32% of medium- to large-budded cells showed extended spindles (1.25-fold decrease, $p = 0.10$). Thus, loss of *Exo*1 significantly delays *rad53* spindle extension in HU.

Artificial Ks at sites distant from ORIs delay *rad53* spindle extension in HU

In light of our observations, we sought to devise an experiment to test whether transferring *CEN*s from early to late replicating genome regions would suffice to bypass the role of Rad53 in restraining spindle extension in HU. Our approach was based on the finding that assembly of an artificial K (AK) can be directed by integrating bacterial operator sequences at desired locations, followed by production of the outer K proteins Ask1 or Dam1 fused to the corresponding bacterial repressor (Kiermaier *et al.*, 2009; Lacefield *et al.*, 2009). LacO-based AK targeting constructs were integrated at sites on chromosomes 2, 9, 10, and 13 ~20 kbp distant from unchecked *ORI*s that fire in both HU-treated WT cells and *rad53* mutants (Figure 9A; Supplemental Figures S6, S7, and S8B). Cells were then transformed with a plasmid encoding Ask1 fused to LacI to induce AK assembly (Lacefield *et al.*, 2009). WT and *rad53* transformants harboring all four AK insertions (4× *LATE-AK*), transformed with vector or p*ASK1-LacI*, were released into HU. After 90 min, spindle lengths were measured and correlated with bud circumference. We observed that activation of the four AKs imposed a reproducible and significant ($p < 0.001$ for three experiments) reduction in *rad53* spindle extension in HU (Figure 9B and Supplemental Figure S8C). In particular, small- to medium-budded *rad53* 4X *LATE-AK* cells expressing *ASK1-LacI* exhibited an average of 10% spindle extension compared with an average of 40% for vector controls (fourfold reduction, red diamonds, Figure 9B and Supplemental Figure S8C). These observations suggest that a limited number of AKs, inserted into sites that are unlikely to replicate in HU during the period of spindle assembly, can significantly offset spindle extension in HU-treated *rad53* mutants.

DISCUSSION

Three principal findings arise from this study. First, the C-motif of Dbf4 plays a novel role in the K-directed pathway specifying early firing of *CEN*-proximal *ORI*s. Second, our data indicate *rad53* spindle extension in HU is a consequence of replication fork catastrophes in proximity to *CEN*s. This has a bearing on how Rad53 effector functions are organized within the S phase checkpoint. Third, while K-MT attachments are required to prevent S phase spindle extension, *CEN* duplication, and thus the capacity for amphitelic K attachments, does not appear to be essential. This finding necessitates a partial revision of our previous model (Bachant *et al.*, 2005) for how spindle extension is restrained at the S phase checkpoint.

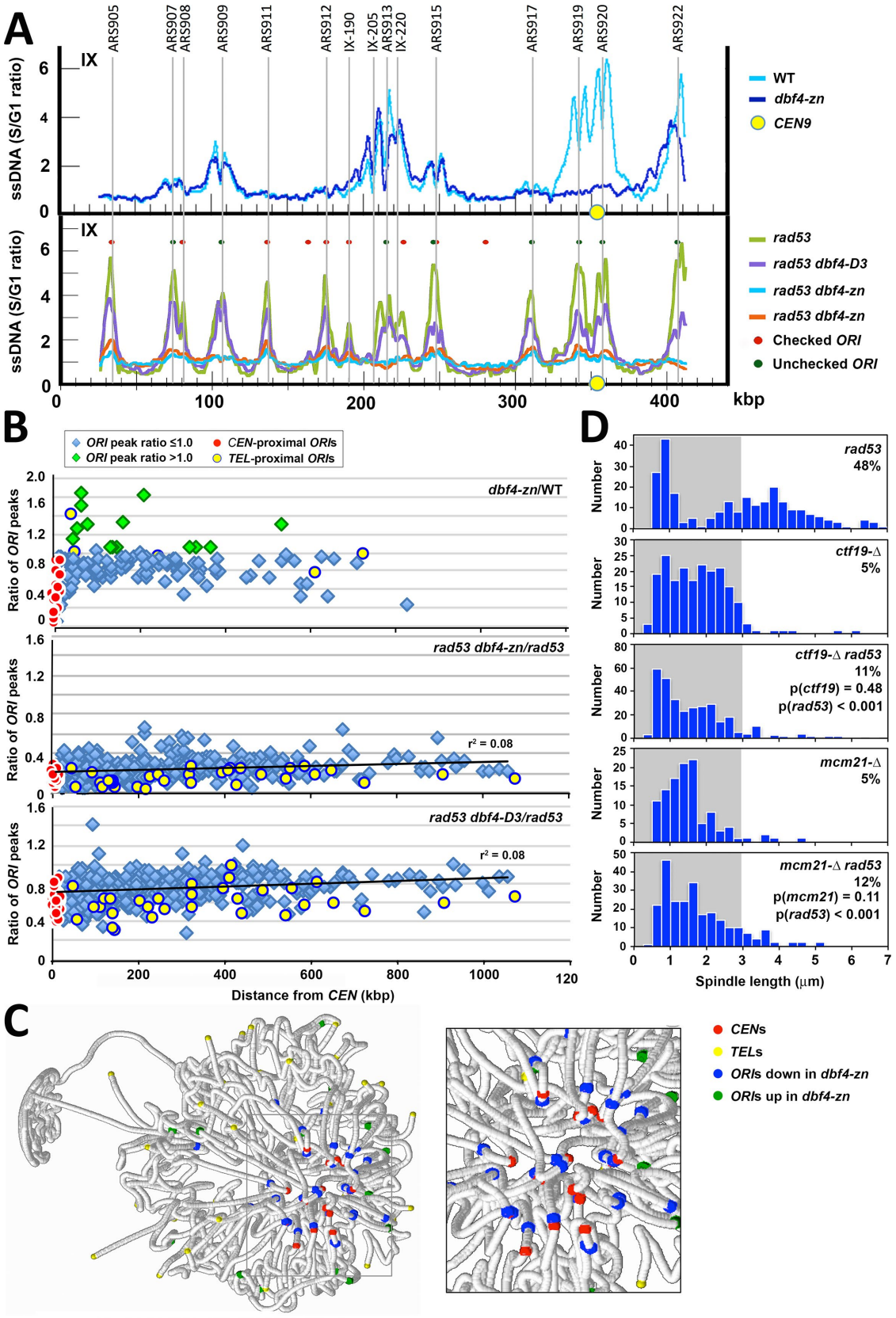

FIGURE 6: *ORI* firing in HU-treated p*dbf4-zn* and *rad53* p*dbf4-zn* mutants. *dbf4-Δ*/p*DBF4* (WT on figure; JJY108), *dbf4-Δ*/p*dbf4-zn* (*dbf4-zn* on the figure; JJY181), *rad53-21 dbf4-Δ*/p*DBF4* (*rad53* on the figure; JJY023), *rad53-21 dbf4-Δ*/p*dbf4-zn* (*rad53 dbf4-zn* on the figure; JJY182), and *rad53-21 dbf4-Δ*/p*dbf4-D3* (*rad53 dbf4-D3* on the figure; JJY029) strains were arrested in G_1. The cultures were split with aliquots either released into 200 mM HU at 30°C or retained at the G_1 block. After 60 min, ssDNA replication intermediates were isolated from G_1 and HU-treated samples

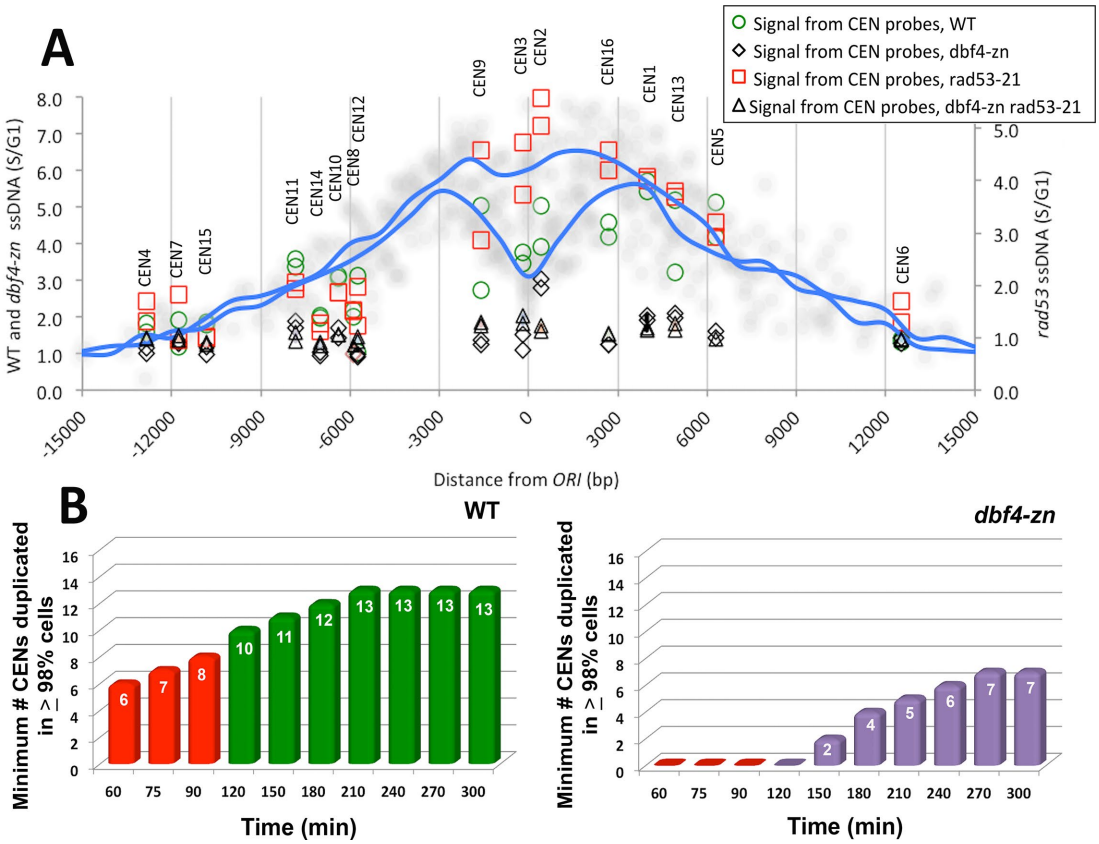

FIGURE 7: Analysis of *CEN* ssDNA and *CEN* duplication in HU. (A) Using the HU replication profiles described in Figure 6, the closest *ORI* to each *CEN* was identified (see also Supplemental Figure S4B; Supplemental Tables S1 and S2). S/G_1 ssDNA values spanning these 16 *ORI*s were determined at 1000-base-pair intervals from the *ORI* center. The average value at each position was used to plot a composite replication profile for the *dbf4-Δ*/p*DBF4* (WT on the *y*-axis) and *rad53-21 dbf4-Δ*/p*DBF4* (*rad53* on the *y*-axis) data sets (blue lines). Data points from each of the 16 individual profiles are also shown (soft gray circles). The split peak characteristic of the WT composite reflects the average extent of bidirectional replication fork movement, while the *rad53* composite appears as a more uniform peak due to accumulation of aberrant ssDNA. Genome arrays used in these experiments have two positions overlapping each *CEN* DNA element. G_1/S ssDNA values for these positions were extracted from the *dbf4-Δ*/p*DBF4* (WT, green circles), *dbf4-Δ*/p*dbf4-zn* (*dbf4-zn*; black diamonds), *rad53-21 dbf4-Δ*/p*DBF4* (*rad53-21*, red squares), and *rad53-21 dbf4-Δ*/p*dbf4-zn* (*dbf4-zn rad53-21*; black triangles) data sets and superimposed on the composite profiles to compare the extent of *CEN* ssDNA in each strain. The relative position of each *CEN* from the center of the composite is shown at the top of the graph. (B) Statistical projections for *CEN* duplication in HU were computed as described in the Supplemental Results. The simulation spans a 60–300 min period following G_1 release into 200 mM HU. The contributions of 45 *CEN*-proximal *ORI*s to *CEN* duplication are included. Graphs display the minimum number of *CEN*s predicted to be duplicated in ≥ 98% of the cell population at the indicated times for *dbf4-Δ*/p*DBF4* (WT) and *dbf4-Δ*/p*dbf4-zn* (*dbf4-zn*). Red columns (60–90 min) denote the period in which the spindle forms in HU. Extending the simulation allows the kinetics and maximal extent of *CEN* duplication to be evaluated.

and hybridized to microarrays. The ratio of S phase (HU) to G_1 hybridization values (S/G_1 ratio) was determined at each array position. (A) Replication profiles for chromosome IX showing reduced firing of *CEN*-flanking ARS919 and ARS920 in p*dbf4-zn* (top profile) and more uniformly reduced *ORI* utilization in *rad53-21* p*dbf4-zn* and *rad53-21* p*dbf4-D3* (bottom profile). (B) *ORI* AUCs were calculated for 177 *ORI* peaks in p*DBF4* (WT) and p*dbf4-zn* strains treated with HU and 403 *ORI* peaks in *rad53-21* p*DBF4* (*rad53*) and *rad53* p*dbf4* strains treated with HU. The ratios of the p*dbf4-zn* to WT *ORI* AUCs, the *rad53* p*dbf4-zn* to *rad53 ORI* AUCs, and the *rad53* p*dbf4-D3* to *rad53 ORI* AUCs (ratio of *ORI* peaks, *y*-axis) were plotted as a function of *ORI* distance to the *CEN*. *CEN* flanking *ORI*s, red circles; *TEL* proximal *ORI*s, yellow circles; *ORI*s with *ORI* AUC ratios ≥1.0, green diamonds. Regression lines are shown for *rad53* plots. (C) p*dbf4-zn ORI*s decreased (blue) or increased (green) by ≥3 SD from the median difference between p*dbf4-zn* and p*DBF4* peak amplitude values are highlighted (RasMol) on a spatial map of the yeast nucleus (see also Supplemental Table S3). Positions of *CEN*s (red) and *TEL*s (yellow) are also shown. Down-regulated *ORI*s in HU-treated p*dbf4-zn* cells tend to be located in close proximity to the *CEN*/SPB cluster, while up-regulated *ORI*s are often located somewhat more distally (inset). (D) The *rad53-21* (JBY2274), *ctf19-Δ* (JBY2250), *ctf19-Δ rad53-21* (JBY2251), *mcm21-Δ* (JBY2327), and *mcm21-Δ rad53-21* (JBY2330) *SPC42-GFP* strains were released from G_1 into 200 mM HU at 30°C. Spindle lengths were measured after 90 min. Percentages of cells with spindles ≥3 µm are shown, along with *p* values (two-tailed *t* test) for indicated comparisons.

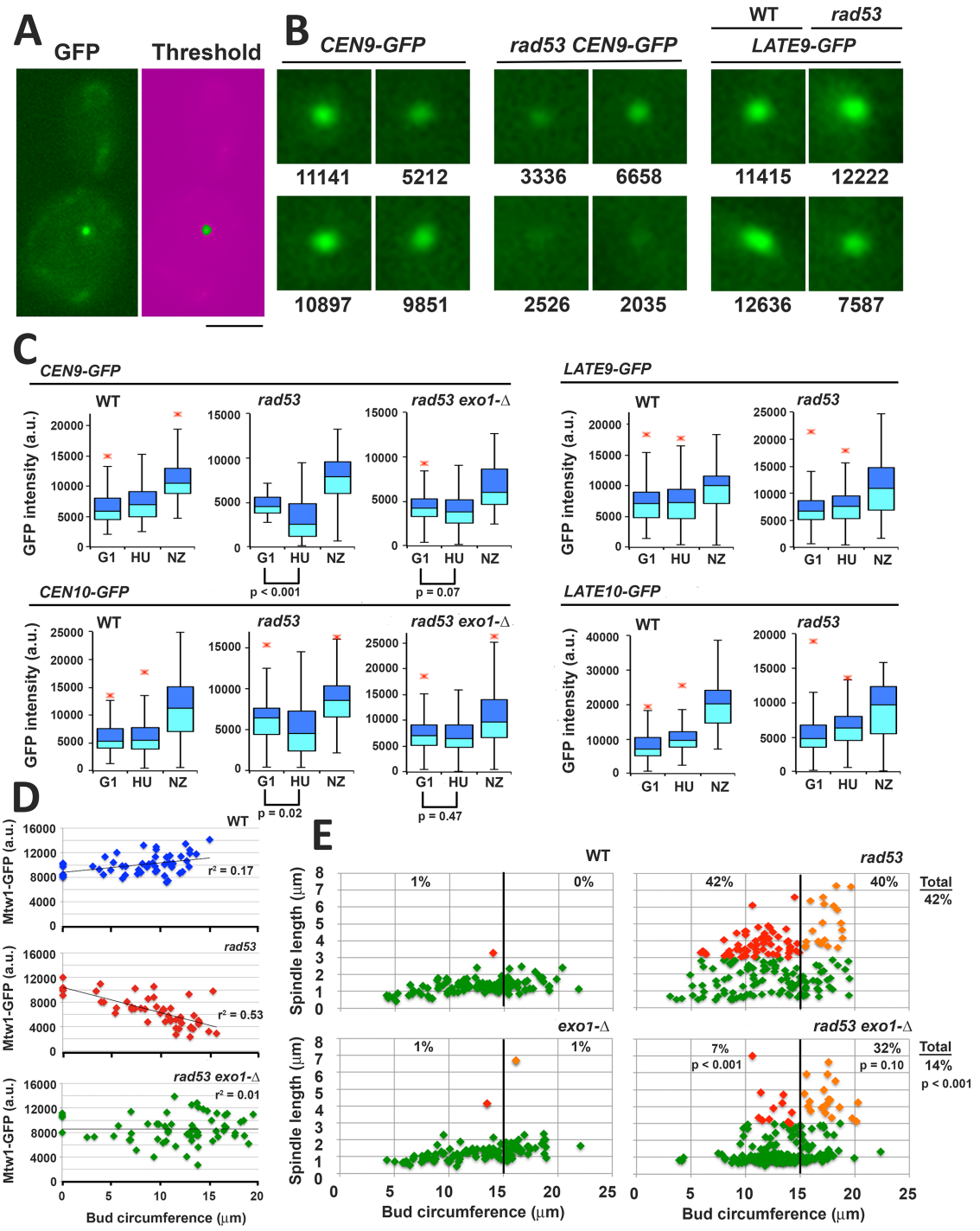

FIGURE 8: *Exo*1 is a determinant of *CEN*/K integrity and spindle extension in HU-treated *rad53* mutants. Strains harboring the indicated GFP chromosome tags were released from G_1 into media containing 200 mM HU or with 15 μg/ml NZ at 30°C: *CEN9-GFP* (WT, JBY2283; *rad53-21*, JBY2295; *exo1-Δ rad53-21*, JBY2299); *CEN10-GFP* (WT, JBY2297; *rad53-21*, JBY2298; *exo1-Δ rad53-21*, JBY2301); *LATE9-GFP* (WT, JBY2289; *rad53-21*, JBY2290); *LATE10-GFP* (WT, JBY2291; *rad53-21*, JBY2293). Cells were processed for microscopy after 90 min. (A) Example of low-end mask to threshold GFP signal. Bar, 4 μm. (B) Representative *CEN9-GFP* and *LATE9-GFP* foci in HU-treated cells, with corresponding intensity values (arbitrary units). (C) Box plots of GFP tag intensities in G_1, HU, and NZ arrested cells. At least 50 cells were analyzed for G_1 and NZ samples; 100 cells were analyzed for HU samples. The *p* values (two-tailed *t* test) are provided in cases where the signal intensity of the HU sample is reduced compared with the G_1 sample. (D) WT (JBY2252), *rad53-21* (JBY2253), and *exo1-Δ rad53-21* (JBY2264) *MTW1-GFP* strains were released from G_1 into media containing both HU and NZ at 30°C. NZ was included so that Ks were not dispersed by spindle extension, facilitating quantification of Mtw1-GFP. After 90 min, live cell mounts were analyzed for Mtw1-GFP intensity. Bud circumference was measured as a proxy for time post-G_1 release. Cells that did not leave the G_1 block were scored to provide a signal baseline. Regression lines and fit estimates are indicated. (E) WT (JBY1129), *rad53-21* (JBY1274), *exo1-Δ* (JBY2246), and *exo1-Δ rad53-21* (JBY2303) *SPC42-GFP* strains were treated with HU as in A and evaluated for bud

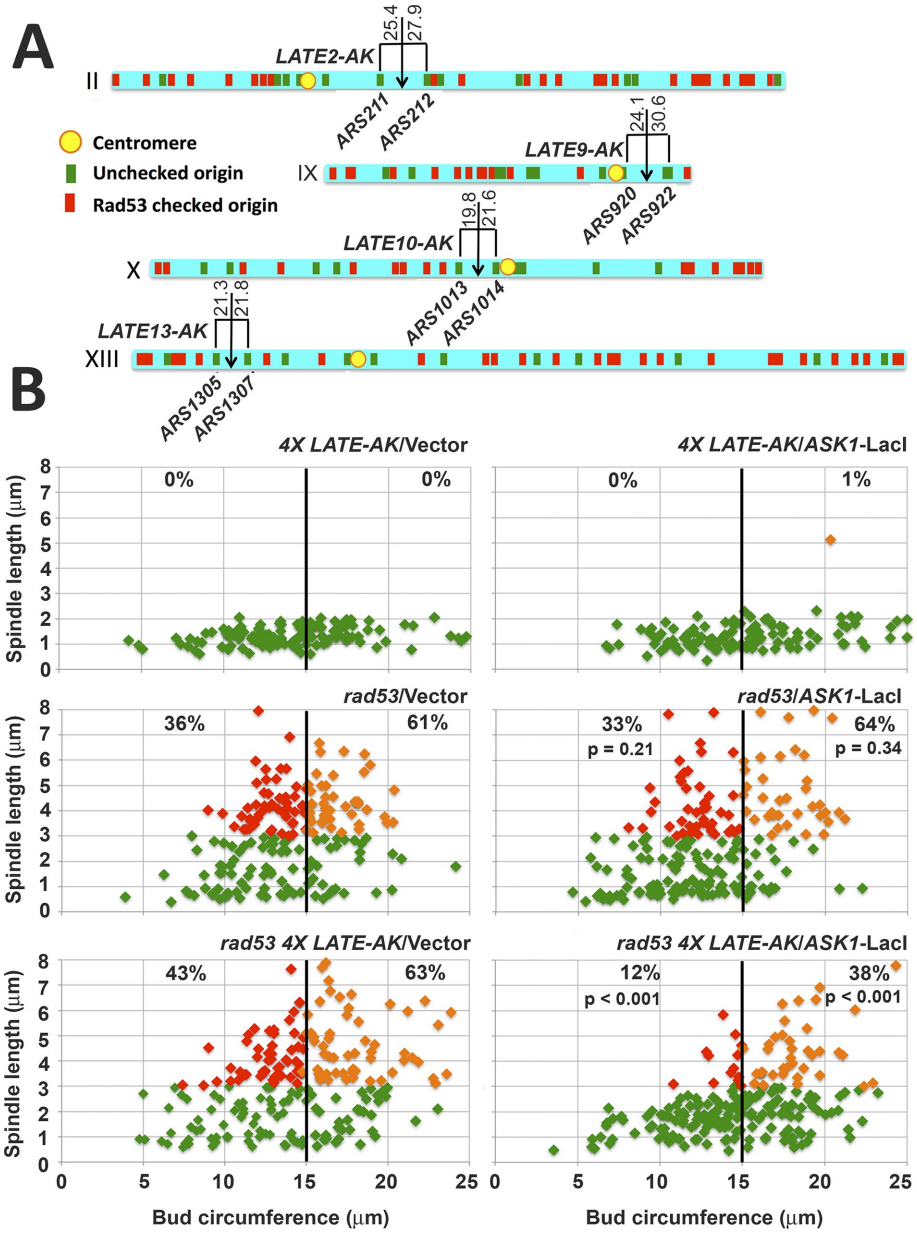

FIGURE 9: AKs at late replicating sites offset *rad53* spindle extension in HU. (A) *AK* insertion sites on chromosomes 2, 9, 10, and 13 are illustrated by downward arrows. Distances to flanking *ORI*s (kbp), as well as positions of unchecked *ORI*s (green), checked *ORI*s (red) and *CEN*s (yellow) are indicated. (B) *RAD53 SPC42-GFP* (JBY2271) and *rad53-21 SP42-GFP* (JBY2273) strains harboring all four *LATE-AK* insertions (*4X LATE-AK*) were transformed with a vector control or a plasmid expressing *ASK1-LacI* to activate synthetic K activity. A *rad53-21 SPC42-GFP* strain (JBY1274) lacking *4X LATE-AK* was similarly transformed. Small colonies emerging on transformation plates were resuspended in liquid media, arrested in G_1, and released into 200 mM HU. After 90 min, cells were analyzed for bud circumference and spindle length. Color scheme for graphs is as described for Figure 8E. The percentages of small/medium and medium/large budded cells with extended spindles are shown in the corresponding regions of the graphs. The *p* values (two-tailed *t* tests) compare spindle extension in *rad53/pASK1-LacI* and *rad53 4X LATE-AK/pASK1-LacI* transformed samples with corresponding vector controls.

The Dbf4 Zn^{2+} finger/C-motif stimulates firing of CEN proximal ORIs

In the K-directed pathway, Dbf4 localizes to the Ctf19/COMA complex and is then transferred to adjacent *ORI*s, leading to accumulation of limiting replication factors (Natsume *et al.*, 2013; Hinshaw *et al.*, 2017). Possible roles for the Dbf4 C-motif are therefore to bind Ctf19/COMA to facilitate DDK recruitment to the K, or to bind components of pre-RCs to facilitate *ORI* transfer. In particular, a *dbf4-zn* defect in the transfer step might increase local DDK availability to regions that are peripheral to the *CEN ORI* cluster, consistent with the increased utilization of some adjacent, less efficient *ORI*s observed in our study. A different possibility is that the C-motif facilitates firing of *CEN*-proximal *ORI*s by stimulating DDK activation of MCM (Harkins *et al.*, 2009; Jones *et al.*, 2010). Positively charged residues flanking the Dbf4 C-motif have been proposed to mediate recognition of priming phosphorylation events (Hughes *et al.*, 2012), and both Mec1 and S phase forms of Cdk1 have been implicated in phosphorylating chromatin-bound MCM to facilitate DDK targeting (Nougaréde *et al.*, 2000; Randell *et al.*, 2010) Speculatively, the R701G mutation in the p*dbf4-D3* allele, which has a less severe effect on *ORI* firing compared with p*dbf4-zn*, could impair such targeting interactions. We note that the Dbf4 C-terminus has previously been implicated in controlling a different group of *ORI*s where early firing is conferred through binding of the Forkhead (Fkh) transcription factors Fkh1 and Fkh2 (Knott *et al.*, 2012; Fang *et al.*, 2017). This suggests the C-motif is acting through at least two pathways to specify early *ORI* firing timing.

In *rad53-21 Δdbf4/pdbf4-zn* mutants, activation of all *ORI*s in HU—both unchecked *ORI*s that fire in *Δdbf4/pdbf4-zn* and *rad53-21 Δdbf4/pDBF4* mutants and checked *ORI*s activated in *rad53-21 Δdbf4/pDBF4*—is greatly reduced. The basis for this synergism is unclear. It is possible that in HU-treated *rad53-21 Δdbf4/pdbf4-zn* mutants, overall DDK activity is reduced below a threshold necessary to fire ~400 *ORI*s throughout the genome, leading to a diminishment at all *ORI*s. Alternatively, Rad53 may function in parallel with the DDK in distinct aspects of

circumference and spindle length. Color coding: cells with spindles <3 μm, green; cells with spindles ≥3 μm and bud circumferences <15 μm (small to medium budded cells), red; cells with spindles ≥3 μm and buds ≥15 μm (medium to large budded cells), orange. The percentages of small/medium and medium/large budded cells with extended spindles are shown on the corresponding regions of the graphs. The total percentage *rad53* and *rad53 exo1* cells with extended spindles is shown on the right-hand side of the graphs. The *p* values (two-tailed *t* tests) compare differences in spindle extension between the *rad53* and *rad53 exo1* data sets.

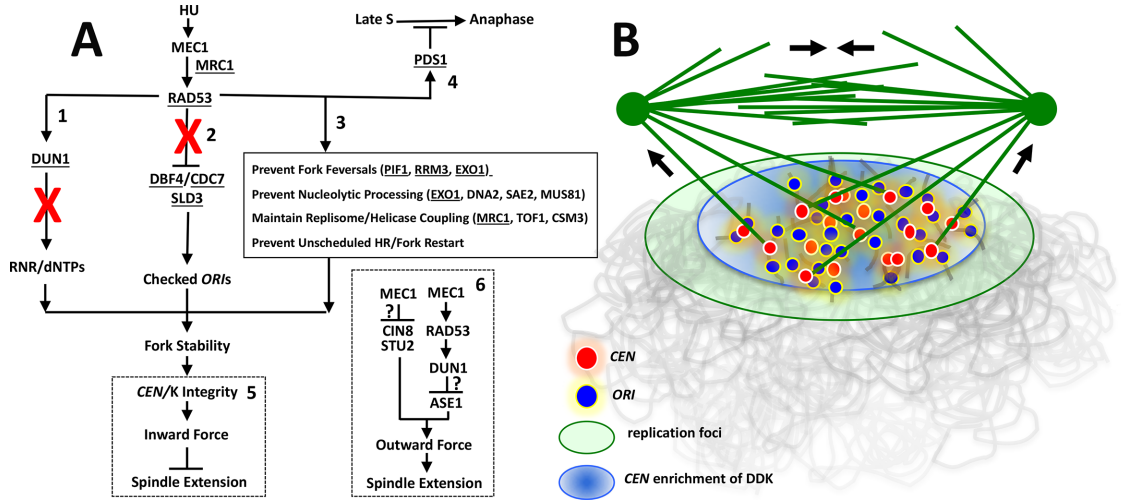

FIGURE 10: Organization and mechanism of the S phase checkpoint block to spindle extension. (A) Checkpoint organization. Six effector pathways relevant to this work are depicted. Rad53 substrates are underlined. See main text for relevant citations. (1) Rad53 activation of Dun1 controls expansion of dNTP pools through transcriptional and posttranslational regulation of RNR. (2) Rad53 inhibition of Dbf4 and Sld3 blocks firing of checked *ORI*s. (3) Rad53 acts directly at replication forks (box) to maintain fork structure. Pathways 1–3 work synergistically to ensure fork progression during replication stress. (4) Rad53 controls a Pds1-dependent cell cycle arrest response that becomes operative in late S phase. (5) We propose the role of Rad53 in stabilizing forks ensures early-replicating *CEN* regions are not subjected to nucleolytic degradation, preserving *CEN*/K integrity and chromosome attachment to the spindle. These attachments generate inward force to restrain spindle extension. (6) Checkpoint regulators also appear to work through additional pathways to down-regulate outward-directed spindle force. Question marks indicate how the checkpoint mediates these responses is not yet clear. Red Xs in 1 and 2 indicate responses crippled downstream of Rad53 in a *dun1-Δ dbf4-m25 sld3-38A* mutant. (B) Proposed S phase spindle structure. DDK activation of *ORI* firing leads to incorporation of *CEN* proximal *ORI*s (blue) and *CEN*s (red) into replication foci (green oval). DDK enrichment at the *CEN ORI* cluster is also depicted (light blue oval). A central assumption is that replicating *CEN*s associated with these structures are partially immobilized, forming a cluster of spindle attachment sites capable of resisting K-MT pulling force (force arrows directed toward SPBs). A distribution of such attachments to both spindle poles could offset spindle extension (force arrows in central spindle) at a characteristic S phase spindle length. Such a spindle assembly intermediate may transiently form during conditions that perturb the relative timing of SPB separation and spindle assembly with completion of S phase. In the illustration, the spindle is depicted as "reaching down" to connect to Ks assembled on immobilized *CEN*s. This is a diagrammatic convenience, as the spindle actually extends through the nucleoplasm and would therefore be emmeshed within the replicating chromatin environment.

ORI firing, with loss of both activities producing a synthetic phenotype (Dohrmann and Sclafani, 2006; Holzen and Sclafani, 2010).

The block to spindle extension in HU is coupled to Rad53 regulation of replication fork stability

As shown in Figure 10A, our findings support an organization of Rad53 effector functions within the S phase checkpoint such that the initial, Pds1-independent, block to spindle extension is coupled to regulation of DNA replication fork stability. First, mutations affecting the DDK (p*dbf4-zn*, p*dbf4-C* alleles), MCM (*mcm2-1*, *mcm3-1*, *mcm5-1*), or K components that specify *CEN ORI* firing (*ctf19-Δ*, *mcm21-Δ*) rescue *rad53* spindle extension in HU. Second, overproduction of Dbf4, which forces some checked *ORI*s to fire in HU (Tanaka *et al.*, 2011), induces spindle extension. Third, Dbf4 and Sld3 are Rad53 substrates that mediate the block to spindle extension, a role that also involves Dun1. Fourth, loss of *Exo1* ameliorates *CEN*/K integrity in HU-treated *rad53* mutants and significantly delays spindle extension. Thus, a sequence of events to explain spindle extension in HU is that, in WT cells and *rad53* mutants, unchecked *ORI*s, including *CEN*-flanking *ORI*s, fire normally. In *rad53* cells, however, unrestrained *ORI* firing, combined with failure to upregulate RNR and misregulation of fork modifying activities, results in pathological fork structures that allow nuclease access to replication forks (Figure 10A, pathways 1–3; Chen *et al.*, 2007; Naylor *et al.*, 2009; Lopez-Mosqueda *et al.*, 2010; Zegerman and Diffley, 2010; Hu *et al.*, 2012; Rossi *et al.*, 2015; Chappidi *et al.*, 2019), leading to a loss of *CEN* DNA integrity in a manner proportional to *CEN* distance from *ORI*s (X^{ed} *CEN*s in Supplemental Figure S9). Based on our analysis of Mtw1-GFP, loss of *CEN* integrity likely corresponds with a *cis*-acting defect in K assembly, which we argue is a proximal cause of spindle extension in HU. As mentioned in the *Introduction*, Rad53 also enforces a later-acting, Pds1-dependent, cell cycle arrest response in HU-treated cells (Figure 10A, pathway 4). This response becomes operative once HU replication stress has been largely circumvented, and likely significantly overlaps Rad53 activity in the DNA damage checkpoint (Gardner *et al.*, 1999; Sanchez *et al.*, 1999; Agarwal *et al.*, 2003), involving stabilization of Pds1, modulation of Cdk1, and regulation of the mitotic exit network (Stueland *et al.*, 1993; Clarke *et al.*, 2001; Palou *et al.*, 2015; Zhou *et al.*, 2016; Zhang *et al.*, 2017).

If spindle extension in HU-treated *rad53* mutants is, in essence, a byproduct of defective DNA replication control, a significant issue concerns whether restraint of spindle extension can be considered a specific checkpoint response that contributes to tolerating DNA replication stress. Insight into this comes from a consideration of *mrc1* mutants, which display an identical spindle extension phenotype in HU to *rad53* strains (Alcasabas *et al.*, 2001). A key difference, however, is that within 30 min HU-treated *mrc1* mutants activate

Rad53 due to rerouting the checkpoint signal through the DNA damage checkpoint mediator Rad9 (Alcasabas *et al.*, 2001; Osborn and Elledge, 2003). *mrc1* mutants survive HU challenge to a much greater extent than *rad53* mutants (Alcasabas *et al.*, 2001) and are able to reform normal preanaphase spindles and biorient duplicated *CEN*s during HU recovery (J.B., unpublished observation). In contrast, *rad53* strains fail in biorientation when HU is removed, a defect that persists despite eventual recovery of *CEN* and bulk genome duplication (Feng *et al.*, 2009). These considerations suggest premature spindle extension in HU is not, in and of itself, necessarily an irrecoverable or lethal checkpoint defect. Rather, our data suggest that spindle extension in HU can be viewed as an early manifestation of a replication-associated perturbation to *CEN* function. If the underlying *CEN* defect is not ameliorated, it ultimately leads to terminal chromosome attachment and/or alignment errors.

S phase spindle structure

Two models have been proposed to explain how Rad53 prevents spindle extension in HU (Figure 10A, pathways 5 and 6). In one, checkpoint signaling down-regulates at least three spindle proteins (Cin8, Stu2, and Ase1; Krishnan *et al.*, 2004; McKnight *et al.*, 2014) that produce or contribute to MT-sliding forces that extend the central spindle (Hoyt *et al.*, 1992; Severin *et al.*, 2001a; Schuyler *et al.*, 2003). Cin8 and Stu2 abundance was found to decline in HU, associated with reduced Cin8 and Stu2 stability and reduced *STU2* transcript accumulation (Krishnan *et al.*, 2004). This depletion required Mec1, suggesting a role for the checkpoint in limiting spindle extension. In a different study, it was found that HU-treated cells preferentially utilize an intragenic transcription start site within *ASE1*, resulting in an Ask1 isoform lacking MT bundling activity (McKnight *et al.*, 2014). This regulation required Rad53, again suggesting checkpoint dampening of spindle extension. Regulation of gene expression through the Mec1-Rad53-Dun1 axis is complex, involving transcriptional and posttranscriptional mechanisms (Jaehnig *et al.*, 2013; Corcoles-Saez *et al.*, 2018; Gay *et al.*, 2018), and specific checkpoint mechanisms controlling Cin8, Stu2, and Ase1 remain to be defined (Figure 10A, question marks in pathway 6). Rad53 inhibition of Ndd1 has been shown to down-regulate G_2/M-expressed genes, including *ASE1* (Edenberg *et al.*, 2014; Yelamanchi *et al.*, 2014); whether this is related to control of *ASE1* intragenic transcription is unclear.

In comparison, the model arising from our previous work sought to explain the requirement for the K in stabilizing spindle structure in HU, leading us to propose that precocious amphitelic K attachments prevented spindle extension during an extended S phase (Bachant *et al.*, 2005). Based on the statistical modeling presented here, at the time HU-treated *rad53* cells exhibit spindle extension, ≥98% of WT cells will have duplicated at least 4–8 *CEN*s. As proposed, biorientation of these duplicated *CEN*s, likely in the context of ongoing replication rather than the C-loop, could contribute to spindle force balance. However, *dbf4-Δ/pdbf4-zn* mutants assemble short spindles in HU even though reduced firing of *CEN*-proximal *ORI*s greatly delays *CEN* duplication. Moreover, in the case of *rad53* mutants, the proximity of *CEN*s to early *ORI*s clearly becomes a liability. Reducing *ORI* firing in the vicinity of *CEN*s, or, conversely, placing AKs at late replicating sites, corresponds with rescue of spindle extension. In comparison, *ddk* mutants that are globally defective in *ORI* firing exhibit a reductional anaphase in HU. Thus, initiating DNA synthesis and *CEN*/K integrity, but not *CEN* duplication, are minimal preconditions to restrict HU spindle extension.

A revised model (Figure 10B and Supplemental Figure S9) to accommodate these findings arises from observations that the movement of interphase chromosomes becomes constrained in S phase (Heun *et al.*, 2001), corresponding with coalescence of *ORI*s into large replication assemblages (Kitamura *et al.*, 2006; Natsume *et al.*, 2013). During this time, Ks remain coupled to MTs, detaching for 1–2 min as they spool through replication foci (Kitamura *et al.*, 2007). On detachment, *CEN*s recoil away from SPBs, and, following duplication and reattachment, are pulled back. These dynamics raise the possibility that replicating *CEN*s are immobilized in a manner that provides resistance to K-MT pulling. Thus, as envisioned in Figure 10B and Supplemental Figure S9, as interdigitating MTs within the forming spindle push SPBs apart, a distribution of monopolar K-MT attachments to both poles could limit extension when S phase is slowed in HU, establishing a distinct force regime/length regulation setpoint for the early S phase spindle. Achieving this distribution would likely require Ipl1, consistent with the role for Ipl1 in preventing HU spindle extension we documented previously (Bachant *et al.*, 2005). In addition to preventing fork catastrophes, a role for Rad53 could also be to stabilize the replication structures proposed to immobilize *CEN*s (Meister *et al.*, 2007). Furthermore, as resistance to extension may be limited, complementary checkpoint responses dampening extension could also be involved. As S phase continued in HU, spindle stability would become increasingly reliant on amphitelic K attachments, the tensile properties of the C-loop, and a checkpoint block to Pds1 proteolysis (Supplemental Figure S9). To our knowledge this is a novel proposal, with implications for budding yeast spindle and karyotype evolution. It suggests that the spindle is a remarkably flexible structure, where tensegrity principles can be accommodated through diverse mechanisms.

MATERIALS AND METHODS

Yeast strains and culture

All *Saccharomyces cerevisiae* strains were derived from the W303-related CRY1 strain (Allen *et al.*, 1994) and are listed in Supplemental Table S6. A list of episomal and integrating plasmids used in this study is provided in Supplemental Table S7. Cells were cultured in standard formulations of yeast extract/peptone/dextrose (YPD) and synthetic complete minimal (SC) media, with 2% glucose or 2% galactose as a carbon source. For G_1 synchronization, α-factor (Bio-Synthesis Corp.) was used at 10 μg/ml. For liquid media, HU was used at 200 mM and NZ was used at 15 μg/ml in YPD. HU and NZ were purchased from Sigma-Aldrich. The 5-fluoroorotic acid (5-FOA) was purchased from Biovectra/Fisher and used at 1 mg/ml. G418 was purchased from Mediatech/Fisher and used at 200 μg/ml in YPD.

Microscopy

Cultures for microscopy were supplemented with 50 μg/ml adenine to quench autofluorescence. For visualizing spindles by α-tubulin immunofluorescence, cells were fixed 4 h in 3.7% formaldehyde; permeabilized in 70% ethanol; spheroplasted for 1 h in 1.2 M sorbitol, 100 mM KPO_4 (pH 7.5), and 50 μg/ml Zymolyase 100T at 37°C; and stained using a 1:50 dilution of YOL1/34 (Accurate Scientific) and a 1:100 dilution of FITC–conjugated α-rat antibodies (Sigma). 4′,6-Diamidino-2-phenylindole (DAPI) staining was performed using Vecta-Shield (Vector Laboratories) containing 10 μg/ml DAPI. To visualize GFP chromosome tags and Spc42-GFP, cells were fixed in 1% formaldehyde for 1.5 min and washed into phosphate-buffered saline. Mtw1-GFP and Tub1-GFP were visualized as live mounts. Cells were visualized on either Nikon E-800 or Nikon Eclipse 80i microscopes equipped with florescence optics and 100× (Plan Apo, 1.40 NA) or 60× (Plan Apo, 1.40 NA) objectives. Spindle length and bud circumference measurements were performed using the MetaMorph (Molecular Devices) suite of software tools. GFP

chromosome tag and Mtw1-GFP intensity measurements were performed by first capturing images of specimens. A low-end mask was then applied using MetaMorph image processing features. The mask was adjusted until only the chromosome tag to be measured remained above the low-end threshold value. The fluorescent tag was then defined as a region, and the integrated intensity value of the region was used as the intensity measurement.

Flow cytometry

DNA content of 95% ethanol-fixed yeast samples was analyzed by prodium idodide staining, followed by flow cytometry using a Becton Dickinson FACSort instrument as previously described (Schober-Ditmore and Bachant, 2000).

ssDNA isolation, hybridization, and analysis

Genome-wide replication profiling by ssDNA labeling was performed as previously described (Peng *et al.*, 2014). Briefly, cells were released from a G_1 block (G_1 control sample) into media containing 200 mM HU for 60 min (S phase sample). Cells from the G_1 control and S phase samples were embedded in agarose plugs for spheroplasting, followed by Klenow (3′-5′ *exo*-)-assisted ssDNA labeling without denaturation of the template DNA. The labeling was done such that the DNA from the G_1 and S samples were differentially decorated with Cy5– and Cy3–conjugated dUTPs, respectively, which were then pooled and cohybridized onto the Agilent 4 × 44 K ChIP-to-chip yeast microarray (G4493A). The ratio of fluorescence intensity from the S sample to that from the G1 sample was calculated and normalized as a "ratio of ssDNA" as previously described (Peng *et al.*, 2014).

Superimposition of insertion sites onto the yeast 3C nuclear model

The coordinates from a three-dimensional model of the yeast genome (Duan *et al.*, 2010) were downloaded from the W. Noble lab website (https://noble.gs.washington.edu/proj/yeast-architecture/sup.html). The coordinates for unchecked origins, checked origins, and K-insertions were transformed from the original atom designation, "C," to "P," "S," and "H," respectively, in the modified visualization script. Visualization was performed with the Rasmol software (windows version Raswin 2.7.5.1, www.openrasmol.org/OpenRasMol.html).

Construction and expression of *dbf4* mutant alleles

The *dbf4-C22*, *dbf4-D3*, and *dbf4-D45* alleles were isolated by screening a PCR mutagenized plasmid library for clones that could partially suppress the temperature sensitivity of *dbf4-1* mutants (Khalil *et al.*, 2007). The *DBF4* insert in these constructs was PCR amplified using JB.83 and JB.84 and included 623 base pairs of upstream promoter sequence and 146 base pairs downstream of the *DBF4* open reading frame:

JB.83: 5′-AGCTCCATGGCATTTTACTTCTCGCAGTACACCG-3′

JB.84: 5′-AGCTGTTAACAGTCAATAGCAAGAAAGTAACAAGGG-3′

Before screening the *dbf4* library, in vivo Cre/lox recombination (Khalil *et al.*, 2007) was used to batch fuse library clones with pHY314, a p*CEN ARS TRP1 lox* yeast episomal vector. The p*dbf4-C22*, p*dbf4-D3*, and p*dbf4-D45* clones were subsequently mobilized to other plasmids, including the p*CEN ARS LEU2 lox(dbf4)lox* constructs used in a number of experiments described in the *Results*, through in vitro Cre/lox recombination (Liu *et al.*, 1998) with target plasmid pJBN242 (p*CEN ARS LEU2 lox(kanMX)lox*).

The *dbf4-zn* allele was constructed by cleaving pJJ019 (p*URA3 DBF4*) at unique *Bsp*E1 and *Swa*I sites within the *DBF4* open reading frame. The *Bsp*EI overhang was made flush with T4 DNA polymerase and ligated to the blunt end of *Swa*I via an intramolecular reaction. The resulting plasmid, pJJ022, contains an 86-base-pair in-frame deletion of the zinc finger region. The *dbf4-zn* was subsequently transferred to other yeast episomal vectors via standard subcloning procedures. The *dbf4-zn* was targeted for integration by cleaving pJJ022 (and pJJ019 as a *DBF4* control) at a unique *Psp*XI site within the promoter. The linearized fragments were looped in through homologous recombination at the corresponding promoter site in a Δ*dbf4::kanMX6* strain, placing *dbf4-zn* (and *DBF4*) in the normal 5′ regulatory context of the endogenous locus.

Construction of AK and chromosomal GFP tags

Regions on chromosomes 2, 9, 10, and 13 were selected for AK insertion based on these sites being predicted to be maximally distant from unchecked *ORI*s that fire in both WT and *rad53* mutant cells treated with HU (Supplemental Figures S6 and S7). Assembly of the four AKs was performed by targeting eight copies of the Lac operator sequence (LacO8X) as previously described (Lacefield *et al.*, 2009). In each of the four *LATE-AK* constructs, PCR-amplified fragments (described below) corresponding to the identified insertion sites were cloned into pJBN291, a p*LEU2-LacO8X* integrating plasmid using *Sac*I and *Xho*I sites incorporated into the PCR primers. Restriction enzyme sites used to linearize the LacO8X plasmids for targeting, as well as the structure of each recombinant, are diagrammed in Supplemental Figure S7. Additional information regarding sequences or PCR strategies used for verifying accurate insertion of each construct is available on request.

LATE2-AK. A 742-base-pair fragment of chromosome 2 corresponding to base pairs 351419–352184 was amplified using JB.305 and JB.306 and cloned into pJBN291, yielding pJBN316, the final targeting plasmid:

JB.305: 5′-GTCTCTCGAGAATTGATCTATGTTGTAGCTGC-3′

JB.306: 5′-AAAGAGCTCTACTCATTATCGAGAACATATGGC-3′

LATE9-AK. A 664-base-pair fragment of chromosome 9 corresponding to base pairs 380966–381606 was amplified using JB.307 and JB.308. After cloning into pJBN291 to yield pJBN317, *Ahd*I/*Bss*HII (blunt/blunt) and *Sac*I/*Sac*I junctions were used to subclone the targeting insert and LacO sequences into pAK047, yielding pJBN322, the final targeting plasmid. This second cloning step incorporates a kanMX marker for G418 resistance:

JB.307: 5′-TTTAGAGCTCGTAATATAAACTTCTCATATGGC-3′

JB.308: 5′-CTGAAGACTCGAGCTGAGTGAGCCG-3′

LATE10-AK. A 548-base-pair fragment of chromosome 10 corresponding to base pairs 395468–395995 was amplified using JB.309 and JB.310. After cloning into pJBN291 to yield pJBN318, *Ahd*I/*Ahd*I and *Sac*/*Sac* junctions were used to subclone the targeting insert and LacO sequences into pJBN196, yielding the final targeting plasmid pJBN323. The second cloning step incorporates yeast *ADE2* as a selectable marker:

JB.309: 5′-CTGACTCGAGGCATTTCAAGGATCAAAAATGCC-3′

JB.310: 5′-ACGTGAGCTCGATTTGGAAGCGCACTACAAGCG-3′

LATE13-AK. A 578-base-pair fragment of chromosome 13 corresponding to base pairs 115353–115930 was amplified using JB.311 and JB.312. After cloning into pJBN291 to yield pJBN319, *Sal*/*Xho* and *Sac*/*Sac* junctions were used to subclone the targeting insert and LacO sequences into pRS406 (Sikorski and Hieter, 1989), yielding the final targeting plasmid pJBN324. The second cloning step incorporates yeast *URA3* as a selectable marker:

JB.311: 5′-TCCACTCGAGAATTCAACCCTGAAGATCTTCCC-3′

JB.312: 5′-ACCAGAGCTCGTCAATTAGCAAGAATAGTTGCC-3′

To activate AK function, JB.303 and JB.304 were used to amplify an 899-base-pair region of the *ASK1* gene. The PCR primers were positioned to remove the *ASK1* start and stop codons, replacing them with unique *Xho*I and *Eco*RI sites, respectively. The *ASK1* PCR fragment was then cloned into the *Xho*I and *Eco*RI sites of pAFS135 (Straight *et al.*, 1997) to yield pJBN320, creating an in frame C-terminal fusion between *ASK1* and the DNA binding domain of LacI. In pJBN320, the *ASK1-LacI* fusion is expressed under control of the *HIS3* promoter, and a nuclear localization sequence (NLS) is additionally fused in frame at the 3′ end of the LacI sequence. A *Sca*I/*Xba*I fragment from pJBN320, containing entire (*HIS3* promoter-*ASK1-LacI-NLS*) element was cloned into pRS413 (Sikorski and Hieter, 1989), yielding pJBN321, a low-copy episomal vector for expression of the *ASK1-LacI-NLS* fusion. pJBN321 fully complemented the growth defect associated with *ask1-2* and *ask1-3* temperature-sensitive mutants, indicating the *ASK1* fusion encoded by pJBN321 is capable of providing *ASK1* essential function:

JB.303:
5′-GACACAACTCGAGATGGATTCTGCAAGCAAAGAGG-3′

JB.304:
5′-GATCGAATTCTCTATTCGTAGAAAAATGAATGATGG-3′

LATE9-GFP and LATE10-GFP. To create more robust GFP visualization of *LATE9*-GFP and *LATE10-GFP* regions than was provided by 8XLacO insertions, pAFS59 (Straight *et al.*, 1997), a *LEU2*-marked integrating plasmid containing 256 copies of the LacO sequence, was transformed into strains harboring *LATE9-AK-LacO8X-kanMX* and *LATE10-AK LacO8X-ADE2* insertions. Leu^+ transformants were visually screened for robust GFP foci, and, for selected *LATE9-GFP* and *LATE10-GFP* transformants, the expected cosegregation of the linked *kanMX-LEU2* and *ADE2-LEU2* markers was verified by tetrad analysis. For all LacO chromosome tags, foci were visualized using an integrated *GFP-LacI* fusion construct under control of the *HIS3* promoter as previously described (Straight *et al.*, 1997).

CEN2-GFP. A 916-base-pair fragment of chromosome 2 corresponding to base pairs 240348–241260 was amplified using JB.297 and JB.298. *Sac*I and *Xho*I sites included on the primers were used to clone the PCR fragment into the corresponding sites of pJBN164, yielding pJBN334. As depicted in Supplemental Figure S7, pJBN334 was used to target *LacO256X-LEU2* sequences 2552 base pairs to the right side of the SCG midpoint of *CEN2*:

JB.297: 5′-CCAGCTCGAGGATTAACGTGTTCTTCCATAGCC-3′

JB.298: 5′-TACCGAGCTCAACGGAAATAAATCCTCCATCCG-3′

CEN9-GFP. A 770-base-pair fragment of chromosome 9 corresponding to base pairs 353395–354212 was amplified using JB.299 and JB.300. *Sac*I and *Xho*I sites included on the primers were used to clone the PCR fragment into pJBN164, yielding pJBN335. pJBN335 was used to target *LacO256X-LEU2* sequences 1884 base pairs to the left side of the SCG midpoint of *CEN9* (Supplemental Figure S7):

JB.299: 5′-GAAGCTCGAGCAATCGACCGTGATCTTCTACCG-3′

JB.300: 5′-CATAGAGCTCAAGGGTATCTCTGATAGTATCGG-3′

CEN10-GFP. A 711-base-pair fragment of chromosome 10 corresponding to base pairs 438082–438793 was amplified using JB.301 and JB.302. *Sac*I and *Xho*I sites on the primers were used to clone the PCR fragment into pJBN164, yielding pJBN336. pJBN336 was used to target *LacO256X-LEU2* 1992 base pairs to the right side of the midpoint of *CEN10* (Supplemental Figure S7):

JB.301: 5′-TGAACTCGAGCTATAAGATAACATCGGTTACGG-3′

JB.302: 5′-CAAAACACTGTTTCTTCAAGAGCTCATCGC-3′

ACKNOWLEDGMENTS

Portions of this work were supported by a grant to J.B. from the California Cancer Research Coordinating Committee, a National Science Foundation award to C.N., and a National Institutes of Health Pathway to Independence Award (5R00GM08137805) to W.F. We thank D. Clarke for providing critical comments on an early draft of the manuscript and O. Aparicio for useful discussions. Thanks also go to S. Elledge, J. Lechner, A. Murray, B. Sclafani, P. Sorger, B. Stillman, and D. Toczyski for strains and reagents. This work is dedicated to the memory of Tim Ngo.

REFERENCES

Agarwal R, Tang Z, Yu H, Cohen-Fix O (2003). Two distinct pathways for inhibiting pds1 ubiquitination in response to DNA damage. J Biol Chem 278, 45027–45033.

Alcasabas AA, Osborn AJ, Bachant J, Hu F, Werler PJ, Bousset K, Furuya K, Diffley JF, Carr AM, Elledge SJ (2001). Mrc1 transduces signals of DNA replication stress to activate Rad53. Nat Cell Biol 3, 958–965.

Allen JB, Zhou Z, Siede W, Friedberg EC, Elledge SJ (1994). The SAD1/RAD53 protein kinase controls multiple checkpoints and DNA damage-induced transcription in yeast. Genes Dev 8, 2401–2415.

Almawi AW, Matthews LA, Larasati, Myrox P, Boulton S, Lai C, Moraes T, Melacini G, Ghirlando R, Duncker BP, *et al.* (2016). "AND" logic gates at work: crystal structure of Rad53 bound to Dbf4 and Cdc7. Sci Rep 6, 34237.

Bachant J, Jessen SR, Kavanaugh SE, Fielding CS (2005). The yeast S phase checkpoint enables replicating chromosomes to bi-orient and restrain spindle extension during S phase distress. J Cell Biol 168, 999–1012.

Bermejo R, Capra T, Jossen R, Colosio A, Frattini C, Carotenuto W, Cocito A, Doksani Y, Klein H, Gómez-González B, *et al.* (2011). The replication checkpoint protects fork stability by releasing transcribed genes from nuclear pores. Cell 146, 233–246.

Bouck DC, Bloom K (2007). Pericentric chromatin is an elastic component of the mitotic spindle. Curr Biol 17, 741–748.

Bousset K, Diffley JFX (1998). The Cdc7 protein kinase is required for origin firing during S phase. Genes Dev 12, 480–490.

Byers B, Goetsch L (1974). Duplication of spindle plaques and integration of the yeast cell cycle. Cold Spring Harb Symp Quant Biol 38, 123–131.

Chappidi N, De Gregorio G, Ferrari S (2019). Replication stress-induced Exo1 phosphorylation is mediated by Rad53/Pph3 and Exo1 nuclear localization is controlled by 14-3-3 proteins. Cell Div 14, 1.

Chen S, Smolka MB, Zhou H (2007). Mechanism of Dun1 activation by Rad53 phosphorylation in Saccharomyces cerevisiae. J Biol Chem 282, 986–995.

Chen Y-C, Kenworthy J, Gabrielse C, Hanni C, Zegerman P, Weinreich M (2013). DNA replication checkpoint signaling depends on a Rad53-Dbf4 N-terminal interaction in Saccharomyces cerevisiae. Genetics 194, 389–401.

Ciosk R, Zachariae W, Michaelis C, Shevchenko A, Mann M, Nasmyth K (1998). An ESP1/PDS1 complex regulates loss of sister chromatid cohesion at the metaphase to anaphase transition in yeast. Cell 93, 1067–1076.

Clarke DJ, Segal M, Jensen S, Reed SI (2001). Mec1p regulates Pds1p levels in S phase: complex coordination of DNA replication and mitosis. Nat Cell Biol 3, 619–627.
Cocker JH, Piatti S, Santocanale C, Nasmyth K, Diffley JF (1996). An essential role for the Cdc6 protein in forming the pre-replicative complexes of budding yeast. Nature 379, 180–182.
Cohen-Fix O, Peters JM, Kirschner MW, Koshland D (1996). Anaphase initiation in Saccharomyces cerevisiae is controlled by the APC-dependent degradation of the anaphase inhibitor Pds1p. Genes Dev 10, 3081–3093.
Colosio A, Frattini C, Pellicanò G, Villa-Hernández S, Bermejo R (2016). Nucleolytic processing of aberrant replication intermediates by an Exo1-Dna2-Sae2 axis counteracts fork collapse-driven chromosome instability. Nucleic Acids Res 44, 10676–10690.
Corcoles-Saez I, Dong K, Johnson AL, Waskiewicz E, Costanzo M, Boone C, Cha RS (2018). Essential function of Mec1, the budding yeast ATM/ATR checkpoint-response kinase, in protein homeostasis. Dev Cell 46, 495–503.e2.
Cotta-Ramusino C, Fachinetti D, Lucca C, Doksani Y, Lopes M, Sogo J, Foiani M (2005). Exo1 processes stalled replication forks and counteracts fork reversal in checkpoint-defective cells. Mol Cell 17, 153–159.
Desany BA, Alcasabas AA, Bachant JB, Elledge SJ (1998). Recovery from DNA replicational stress is the essential function of the S-phase checkpoint pathway. Genes Dev 12, 2956–2970.
Dohrmann PR, Sclafani RA (2006). Novel role for checkpoint Rad53 protein kinase in the initiation of chromosomal DNA replication in Saccharomyces cerevisiae. Genetics 174, 87–99.
Duan Z, Andronescu M, Schutz K, McIlwain S, Kim YJ, Lee C, Shendure J, Fields S, Blau CA, Noble WS (2010). A three-dimensional model of the yeast genome. Nature 465, 363–367.
Duncker BP, Shimada K, Tsai-Pflugfelder M, Pasero P, Gasser SM (2002). An N-terminal domain of Dbf4p mediates interaction with both origin recognition complex (ORC) and Rad53p and can deregulate late origin firing. Proc Natl Acad Sci USA 99, 16087–16092.
Edenberg ER, Vashisht A, Benanti JA, Wohlschlegel J, Toczyski DP (2014). Rad53 downregulates mitotic gene transcription by inhibiting the transcriptional activator Ndd1. Mol Cell Biol 34, 725–738.
Fang D, Lengronne A, Shi D, Forey R, Skrzypczak M, Ginalski K, Yan C, Wang X, Cao Q, Pasero P, *et al*. (2017). Dbf4 recruitment by forkhead transcription factors defines an upstream rate-limiting step in determining origin firing timing. Genes Dev 31, 2405–2415.
Feng W, Bachant J, Collingwood D, Raghuraman MK, Brewer BJ (2009). Centromere replication timing determines different forms of genomic instability in saccharomyces cerevisiae checkpoint mutants during replication stress. Genetics 183, 1249–1260.
Feng W, Collingwood D, Boeck ME, Fox LA, Alvino GM, Fangman WL, Raghuraman MK, Brewer BJ (2006). Genomic mapping of single-stranded DNA in hydroxyurea-challenged yeasts identifies origins of replication. Nat Cell Biol 8, 148–155.
Feng W, Di Rienzi SC, Raghuraman MK, Brewer BJ (2011). Replication stress-induced chromosome breakage is correlated with replication fork progression and is preceded by single-stranded DNA formation. G3 (Bethesda) 1, 327–335.
Feng W, Raghuraman MK, Brewer BJ (2007). Mapping yeast origins of replication via single-stranded DNA detection. Methods 41, 151–157.
Gardner R, Putnam CW, Weinert T (1999). RAD53, DUN1 and PDS1 define two parallel G2/M checkpoint pathways in budding yeast. EMBO J 18, 3173–3185.
Gay S, Piccini D, Bruhn C, Ricciardi S, Soffientini P, Carotenuto W, Biffo S, Foiani M (2018). A Mad2-mediated translational regulatory mechanism promoting S-phase cyclin synthesis controls origin firing and survival to replication stress. Mol Cell 70, 628–638.e5.
Hardy CFJ, Dryga O, Seematter S, Pahl PMB, Sclafani RA (1997). mcm5/cdc46-bob1 bypasses the requirement for the S phase activator Cdc7p. Proc Natl Acad Sci USA 94, 3151–3155.
Harkins V, Gabrielse C, Haste L, Weinreich M (2009). Budding yeast Dbf4 sequences required for Cdc7 kinase activation and identification of a functional relationship between the Dbf4 and Rev1 BRCT domains. Genetics 183, 1269–1282.
Hartwell LH (1976). Sequential function of gene products relative to DNA synthesis in the yeast cell cycle. J Mol Biol 104, 803–817.
Heun P, Laroche T, Shimada K, Furrer P, Gasser SM (2001). Chromosome dynamics in the yeast interphase nucleus. Science 294, 2181–2186.
Hinshaw SM, Makrantoni V, Harrison SC, Marston AL (2017). The Kinetochore Receptor for the Cohesin Loading Complex. Cell 171, 72–84.e13.
Holzen TM, Sclafani RA (2010). Genetic interaction of RAD53 protein kinase with histones is important for DNA replication. Cell Cycle 9, 4735–4747.
Hoyt MA, He L, Loo KK, Saunders WS (1992). Two Saccharomyces cerevisiae kinesin-related gene products required for mitotic spindle assembly. J Cell Biol 118, 109–120.
Hu J, Sun L, Shen F, Chen Y, Hua Y, Liu Y, Zhang M, Hu Y, Wang Q, Xu W, *et al*. (2012). The intra-S phase checkpoint targets Dna2 to prevent stalled replication forks from reversing. Cell 149, 1221–1232.
Hughes S, Elustondo F, Di Fonzo A, Leroux FG, Wong AC, Snijders AP, Matthews SJ, Cherepanov P (2012). Crystal structure of human CDC7 kinase in complex with its activator DBF4. Nat Struct Mol Biol 19, 1101–1107.
Jackson AL, Pahl PM, Harrison K, Rosamond J, Sclafani RA (1993). Cell cycle regulation of the yeast Cdc7 protein kinase by association with the Dbf4 protein. Mol Cell Biol 13, 2899–2908.
Jaehnig EJ, Kuo D, Hombauer H, Ideker TG, Kolodner RD (2013). Checkpoint kinases regulate a global network of transcription factors in response to DNA damage. Cell Rep 4, 174–188.
Jensen S, Segal M, Clarke DJ, Reed SI (2001). A novel role of the budding yeast separin Esp1 in anaphase spindle elongation: evidence that proper spindle association of Esp1 is regulated by Pds1. J Cell Biol 152, 27–40.
Jones DR, Prasad AA, Chan PK, Duncker BP (2010). The Dbf4 motif C zinc finger promotes DNA replication and mediates resistance to genotoxic stress. Cell Cycle 9, 2018–2026.
Katou Y, Kanoh Y, Bando M, Noguchi H, Tanaka H, Ashikari T, Sugimoto K, Shirahige K (2003). S-phase checkpoint proteins Tof1 and Mrc1 form a stable replication-pausing complex. Nature 424, 1078–1083.
Khalil A-M, Julius JA, Bachant J (2007). One step construction of PCR mutagenized libraries for genetic analysis by recombination cloning. Nucleic Acids Res 35, e104.
Khmelinskii A, Roostalu J, Roque H, Antony C, Schiebel E (2009). Phosphorylation-dependent protein interactions at the spindle midzone mediate cell cycle regulation of spindle elongation. Dev Cell 17, 244–256.
Kiermaier E, Woehrer S, Peng Y, Mechtler K, Westermann S (2009). A Dam1-based artificial kinetochore is sufficient to promote chromosome segregation in budding yeast. Nat Cell Biol 11, 1109–1115.
Kitamura E, Blow JJ, Tanaka TU (2006). Live-cell imaging reveals replication of individual replicons in eukaryotic replication factories. Cell 125, 1297–1308.
Kitamura E, Tanaka K, Kitamura Y, Tanaka TU (2007). Kinetochore microtubule interaction during S phase in Saccharomyces cerevisiae. Genes Dev 21, 3319–3330.
Knott SRV, Peace JM, Ostrow AZ, Gan Y, Rex AE, Viggiani CJ, Tavaré S, Aparicio OM (2012). Forkhead transcription factors establish origin timing and long-range clustering in S. cerevisiae. Cell 148, 99–111.
Krishnan V, Nirantar S, Crasta K, Cheng AYH, Surana U (2004). DNA replication checkpoint prevents precocious chromosome segregation by regulating spindle behavior. Mol Cell 16, 687–700.
Lacefield S, Lau DTC, Murray AW (2009). Recruiting a microtubule-binding complex to DNA directs chromosome segregation in budding yeast. Nat Cell Biol 11, 1116–1120.
Lianga N, Doré C, Kennedy EK, Yeh E, Williams EC, Fortinez CM, Wang A, Bloom KS, Rudner AD (2018). Cdk1 phosphorylation of Esp1/Separase functions with PP2A and Slk19 to regulate pericentric Cohesin and anaphase onset. PLoS Genet 14, a1007029.
Liu H, Liang F, Jin F, Wang Y (2008). The coordination of centromere replication, spindle formation, and kinetochore-microtubule interaction in budding yeast. PLoS Genet 4, e1000262.
Liu Q, Li MZ, Leibham D, Cortez D, Elledge SJ (1998). The univector plasmid-fusion system, a method for rapid construction of recombinant DNA without restriction enzymes. Curr Biol 8, 1300–1309.
Lopes M, Cotta-Ramusino C, Pellicioli A, Liberi G, Plevani P, Muzi-Falconi M, Newlon CS, Foiani M (2001). The DNA replication checkpoint response stabilizes stalled replication forks. Nature 412, 557–561.
Lopez-Mosqueda J, Maas NL, Jonsson ZO, DeFazio Eli LG, Wohlschlegel J, Toczyski DP (2010). Damage-induced phosphorylation of Sld3 is important to block late origin firing. Nature 467, 479–483.
Ma L, McQueen J, Cuschieri L, Vogel J, Measday V (2007). Spc24 and Stu2 promote spindle integrity when DNA replication is stalled. Mol Biol Cell 18, 2805–2816.
Mantiero D, Mackenzie A, Donaldson A, Zegerman P (2011). Limiting replication initiation factors execute the temporal programme of origin firing in budding yeast. EMBO J 30, 4805–4814.
Masai H, Arai K (2000). Dbf4 motifs: conserved motifs in activation subunits for Cdc7 kinases essential for S-phase. Biochem Biophys Res Commun 275, 228–232.

Matthews LA, Selvaratnam R, Jones DR, Akimoto M, McConkey BJ, Melacini G, Duncker BP, Guarné A (2014). A novel non-canonical forkhead-associated (FHA) domain-binding interface mediates the interaction between Rad53 and Dbf4 proteins. J Biol Chem 289, 2589–2599.
McKnight K, Liu H, Wang Y (2014). Replicative stress induces intragenic transcription of the ASE1 gene that negatively regulates Ase1 activity. Curr Biol 24, 1101–1106.
Meister P, Taddei A, Ponti A, Baldacci G, Gasser SM (2007). Replication foci dynamics: replication patterns are modulated by S-phase checkpoint kinases in fission yeast. EMBO J 26, 1315–1326.
Morafraile EC, Diffley JFX, Tercero JA, Segurado M (2015). Checkpoint-dependent RNR induction promotes fork restart after replicative stress. Sci Rep 5, 7886.
Nannas NJ, O'Toole ET, Winey M, Murray AW (2014). Chromosomal attachments set length and microtubule number in the Saccharomyces cerevisiae mitotic spindle. Mol Biol Cell 25, 4034–4048.
Natsume T, Müller CA, Katou Y, Retkute R, Gierliński M, Araki H, Blow JJ, Shirahige K, Nieduszynski CA, Tanaka TU (2013). Kinetochores coordinate pericentromeric cohesion and early DNA replication by Cdc7-Dbf4 kinase recruitment. Mol Cell 50, 661–674.
Navas TA, Zhou Z, Elledge SJ (1995). DNA polymerase epsilon links the DNA replication machinery to the S phase checkpoint. Cell 80, 29–39.
Naylor ML, Li J, Osborn AJ, Elledge SJ (2009). Mrc1 phosphorylation in response to DNA replication stress is required for Mec1 accumulation at the stalled fork. Proc Natl Acad Sci USA 106, 12765–12770.
Nougarède R, Della Seta F, Zarzov P, Schwob E (2000). Hierarchy of S-phase-promoting factors: yeast Dbf4-Cdc7 kinase requires prior S-phase cyclin-dependent kinase activation. Mol Cell Biol 20, 3795–3806.
Osborn AJ, Elledge SJ (2003). Mrc1 is a replication fork component whose phosphorylation in response to DNA replication stress activates Rad53. Genes Dev 17, 1755–1767.
Palou R, Palou G, Quintana DG (2017). A role for the spindle assembly checkpoint in the DNA damage response. Curr Genet 63, 275–280.
Palou G, Palou R, Zeng F, Vashisht AA, Wohlschlegel JA, Quintana DG (2015). Three different pathways prevent chromosome segregation in the presence of DNA damage or replication stress in budding yeast. PLoS Genet 11, e1005468.
Pardo B, Crabbé L, Pasero P (2017). Signaling pathways of replication stress in yeast. FEMS Yeast Res 17, doi: 10.1093/femsyr/fow101.
Peng J, Raghuraman MK, Feng W (2014). Analysis of ssDNA gaps and DSBs in genetically unstable yeast cultures. Methods Mol Biol 1170, 501–515.
Piatti S, Lengauer C, Nasmyth K (1995). Cdc6 is an unstable protein whose de novo synthesis in G1 is important for the onset of S phase and for preventing a "reductional" anaphase in the budding yeast Saccharomyces cerevisiae. EMBO J 14, 3788–3799.
Poli J, Tsaponina O, Crabbé L, Keszthelyi A, Pantesco V, Chabes A, Lengronne A, Pasero P (2012). dNTP pools determine fork progression and origin usage under replication stress. EMBO J 31, 883–894.
Raghuraman MK, Winzeler EA, Collingwood D, Hunt S, Wodicka L, Conway A, Lockhart DJ, Davis RW, Brewer BJ, Fangman WL (2001). Replication dynamics of the yeast genome. Science 294, 115–121.
Randell JCW, Fan A, Chan C, Francis LI, Heller RC, Galani K, Bell SP (2010). Mec1 is one of multiple kinases that prime the Mcm2-7 helicase for phosphorylation by Cdc7. Mol Cell 40, 353–363.
Rossi SE, Ajazi A, Carotenuto W, Foiani M, Giannattasio M (2015). Rad53-mediated regulation of Rrm3 and Pif1 DNA helicases contributes to prevention of aberrant fork transitions under replication stress. Cell Rep 13, 80–92.
Sanchez Y, Bachant J, Wang H, Hu F, Liu D, Tetzlaff M, Elledge SJ (1999). Control of the DNA damage checkpoint by chk1 and rad53 protein kinases through distinct mechanisms. Science 286, 1166–1171.
Sanchez Y, Desany BA, Jones WJ, Liu Q, Wang B, Elledge SJ (1996). Regulation of RAD53 by the ATM-like kinases MEC1 and TEL1 in yeast cell cycle checkpoint pathways. Science 271, 357–360.
Santocanale C, Diffley JF (1998). A Mec1- and Rad53-dependent checkpoint controls late-firing origins of DNA replication. Nature 395, 615–618.
Saunders W, Lengyel V, Hoyt MA (1997). Mitotic spindle function in Saccharomyces cerevisiae requires a balance between different types of kinesin-related motors. Mol Biol Cell 8, 1025–1033.
Schober-Ditmore W, Bachant J (2000). Yeast DNA flow cytometry. In: In Living Color: Protocols in Flow Cytometry and Cell Sorting, ed. RA Diamond and S DeMaggio, New York: Springer Science & Business Media, 455–460.
Schuyler SC, Liu JY, Pellman D (2003). The molecular function of Ase1p: evidence for a MAP-dependent midzone-specific spindle matrix. Microtubule-associated proteins. J Cell Biol 160, 517–528.
Severin F, Habermann B, Huffaker T, Hyman T (2001a). Stu2 promotes mitotic spindle elongation in anaphase. J Cell Biol 153, 435–442.
Severin F, Hyman AA, Piatti S (2001b). Correct spindle elongation at the metaphase/anaphase transition is an APC-dependent event in budding yeast. J Cell Biol 155, 711–718.
Sheu Y-J, Stillman B (2010). The Dbf4-Cdc7 kinase promotes S phase by alleviating an inhibitory activity in Mcm4. Nature 463, 113–117.
Shirahige K, Hori Y, Shiraishi K, Yamashita M, Takahashi K, Obuse C, Tsurimoto T, Yoshikawa H (1998). Regulation of DNA-replication origins during cell-cycle progression. Nature 395, 618–621.
Sikorski RS, Hieter P (1989). A system of shuttle vectors and yeast host strains designed for efficient manipulation of DNA in Saccharomyces cerevisiae. Genetics 122, 19–27.
Sogo JM, Lopes M, Foiani M (2002). Fork reversal and ssDNA accumulation at stalled replication forks owing to checkpoint defects. Science 297, 599–602.
Stephens AD, Haase J, Vicci L, Taylor RM 2nd, Bloom K (2011). Cohesin, condensin, and the intramolecular centromere loop together generate the mitotic chromatin spring. J Cell Biol 193, 1167–1180.
Straight AF, Marshall WF, Sedat JW, Murray AW (1997). Mitosis in living budding yeast: anaphase A but no metaphase plate. Science 277, 574–578.
Stueland CS, Lew DJ, Cismowski MJ, Reed SI (1993). Full activation of p34CDC28 histone H1 kinase activity is unable to promote entry into mitosis in checkpoint-arrested cells of the yeast Saccharomyces cerevisiae. Mol Cell Biol 13, 3744–3755.
Tanaka S, Nakato R, Katou Y, Shirahige K, Araki H (2011). Origin association of Sld3, Sld7, and Cdc45 proteins is a key step for determination of origin-firing timing. Curr Biol 21, 2055–2063.
Tanaka TU, Rachidi N, Janke C, Pereira G, Galova M, Schiebel E, Stark MJR, Nasmyth K (2002). Evidence that the Ipl1-Sli15 (Aurora kinase-INCENP) complex promotes chromosome bi-orientation by altering kinetochore-spindle pole connections. Cell 108, 317–329.
Warsi TH, Navarro MS, Bachant J (2008). DNA topoisomerase II is a determinant of the tensile properties of yeast centromeric chromatin and the tension checkpoint. Mol Biol Cell 19, 4421–4433.
Weinert TA, Kiser GL, Hartwell LH (1994). Mitotic checkpoint genes in budding yeast and the dependence of mitosis on DNA replication and repair. Genes Dev 8, 652–665.
Yamamoto A, Guacci V, Koshland D (1996). Pds1p, an inhibitor of anaphase in budding yeast, plays a critical role in the APC and checkpoint pathway(s). J Cell Biol 133, 99–110.
Yeh E, Haase J, Paliulis LV, Joglekar A, Bond L, Bouck D, Salmon ED, Bloom KS (2008). Pericentric chromatin is organized into an intramolecular loop in mitosis. Curr Biol 18, 81–90.
Yelamanchi SK, Veis J, Anrather D, Klug H, Ammerer G (2014). Genotoxic stress prevents Ndd1-dependent transcriptional activation of G2/M-specific genes in Saccharomyces cerevisiae. Mol Cell Biol 34, 711–724.
Zegerman P, Diffley JFX (2010). Checkpoint dependent inhibition of DNA replication initiation by Sld3 and Dbf4 phosphorylation. Nature 467, 474–478.
Zhang Z, Ren P, Vashisht AA, Wohlschlegel JA, Quintana DG, Zeng F (2017). Cdk1-interacting protein Cip1 is regulated by the S phase checkpoint in response to genotoxic stress. Genes Cells 22, 850–860.
Zhao X, Rothstein R (2002). The Dun1 checkpoint kinase phosphorylates and regulates the ribonucleotide reductase inhibitor Sml1. Proc Natl Acad Sci USA 99, 3746–3751.
Zhong Y, Nellimoottil T, Peace JM, Knott SRV, Villwock SK, Yee JM, Jancuska JM, Rege S, Tecklenburg M, Sclafani RA, *et al.* (2013). The level of origin firing inversely affects the rate of replication fork progression. J Cell Biol 201, 373–383.
Zhou C, Elia AEH, Naylor ML, Dephoure N, Ballif BA, Goel G, Xu Q, Ng A, Chou DM, Xavier RJ, *et al.* (2016). Profiling DNA damage-induced phosphorylation in budding yeast reveals diverse signaling networks. Proc Natl Acad Sci USA 113, E3667–E3675.
Zhou Z, Elledge SJ (1993). DUN1 encodes a protein kinase that controls the DNA damage response in yeast. Cell 75, 1119–1127.

ETOC:

The yeast S phase checkpoint kinase Rad53 is shown to prevent untimely spindle extension in S phase by maintaining replication fork integrity in the vicinity of centromeres, preventing degradation of CEN DNA. However, restraint of spindle extension does not require actual CEN duplication, suggesting a novel S phase intermediate in spindle assembly.